GROWTH AND CHARACTERIZATION OF THERMALLY EVAPORATED ENERGY EFFICIENT COATINGS BASED ON THE TRANSITION METAL OXIDES (CHROMIUM OXIDE, NICKEL OXIDE, MOLYBDENUM OXIDE AND VANADIUM OXIDE)

BY

Syed Haseeb Ali Ahmad

A Thesis Presented to the
DEANSHIP OF GRADUATE STUDIES

KING FAHD UNIVERSITY OF PETROLEUM & MINERALS

DHAHRAN, SAUDI ARABIA

In Partial Fulfillment of the
Requirements for the Degree of

MASTER OF SCIENCE

In

PHYSICS

May 2015

KING FAHD UNIVERSITY OF PETROLEUM & MINERALS

DHAHRAN- 31261, SAUDI ARABIA

DEANSHIP OF GRADUATE STUDIES

This thesis, written by **Syed Haseeb Ali Ahmad** under the direction of his thesis advisor and approved by his thesis committee, has been presented and accepted by the Dean of Graduate Studies, in partial fulfillment of the requirements for the degree of **MASTER OF SCIENCE IN PHYSICS.**

Dr. Mohammad F. Al-Kuhaili
(Advisor)

Dr. S.M.A Durrani
(Co-Advisor)

Dr. Mohammad M. Faiz
(Member)

Dr. Anwar-ul-Hamid
(Member)

Dr. Abdel Karim Mekki
(Member)

3/5/2015

Dr. Abdullah A. Al-Sunaidi
Department Chairman

Dr. Salam A. Zummo
Dean of Graduate Studies

10/5/15

Date

Dedicated to My Parents

ACKNOWLEDGMENT

All the worthy praise to Allah, who never left me alone and grant me courage to accomplish this work successfully. All the peace and blessing on Rasool Allah (ﷺ), who is the blessing for all the worlds.

I would like to express my deepest gratitude to my thesis advisor, Dr. Mohammad Fayyad Al-Kuhaili, for his excellent guidance, caring, patience, and for providing me with an excellent atmosphere for doing research. I have really enjoyed working with him. I am really thankful to him for his kindness, and precious time devoted by him to make the things easier for me during the study and research. I hope the skills, knowledge, and guidance attained by me from him will help me in the future to start my career as an independent researcher.

I would also like to acknowledge all the efforts made by my co-supervisor Dr. Sardar Muhammad Ayub Durrani to make my experiments successful. I am very thankful to him for his guidance, motivation and support throughout my MS study.

Special thanks to my committee members Dr. Muhammad Faiz, Dr. Anwar-ul-Hamid, and Dr. Abdel Karim Mekki for continuous feedback, suggestions, support and encouragement. To learn the X-ray photoelectron spectroscopy was a great challenge for me and was impossible without Dr. Faiz. To study the structure of thin films of nanometer thickness using X-ray diffraction was a difficult task and was not possible without Dr. Hamid. The continuous encouragement and precious suggestion by Dr. Abdel Karim Mekki were indispensable in thesis writing.

I appreciate all efforts and logistic support provided by Mr. Imran Ali Bakhtiari. I am very thankful to him for his support during research and invaluable training on equipment.

King Fahd University of Petroleum and Minerals is also acknowledged for all support and privileges during my MS study in the Physics Department. I am also very thankful to the Chairman and all the staff members of the Physics Department for their support and cooperation.

Finally, I would like to say special thanks to my parents and family for their support during this whole period. Special thanks to my wife (late) who motivated and encouraged me to carry the struggle with life. I would like to express my special thanks to my son for his patience and sacrifice, who missed his parents during this period.

TABLE OF CONTENTS

LIST OF FIGURES

LIST OF TABLES

ABSTRACT

Full Name : Syed Haseeb Ali Ahmad

Thesis Title : Growth and characterization of thermally evaporated energy efficient coatings based on the transition metal oxides(Chromium Oxide, Molybdenum Oxide, Nickle Oxide, Vanadium Oxide)

Major Field : Physics

Date of Degree : May 2015

Transparent heat mirrors (THM) allow the visible range of electromagnetic radiation to transmit through them but reflect the infrared part. In order to realize this potential, the two layer dielectric/metal system was used on different types of substrates. The multilayer thin films were deposited on different substrates using different transitions metal oxides as the dielectrics. The selected metal oxides were chromium oxide (Cr_2O_3), molybdenum oxide (MoO_3), nickel oxide (NiO), and vanadium oxide (V_2O_5) and were deposited by thermal evaporation. Silver (Ag) was used as metal. The surface morphology and structural properties were investigated by atomic force microscopy (AFM) and X-ray diffraction (XRD), respectively. XRD revealed that all the films were amorphous except nickel oxide. The AFM study revealed that the morphology of the surfaces exhibited a columnar structure. The root mean square surface roughness (R_{rms}) of the films indicated smooth surfaces of the metal oxides. The R_{rms} values for the silver films indicated a rough and porous structure. The chemical properties of the individual as well as the two layer structure films were determined using X-ray photoelectron spectroscopy (XPS). The depth profile of THM coatings showed that the interface between the two layers was not sharp, and thus diffusion of the oxide into the silver layer took place. The optical properties of the films such as band gap, absorption coefficient, refractive index, and extinction coefficient were determined from spectrophotometric measurements. The fabricated two layer structures were

highly transparent in visible region and highly reflective in infrared region of electromagnetic spectrum, which exhibited the desired optical properties for transparent heat mirrors applications.

ABSTRACT (ARABIC)

ملخص الرسالة

الاسم الكامل: سّيد حسيب علي أحمد

عنوان الرسالة: تحضير و خصائص الطبقات الحافظة للطاقة المصنوعة من أكاسيد المعادن الانتقالية

التخصص: الفيزياء

تاريخ الدرجة العلمية: مايو 2015

المرايا الشفافة العاكسة للحرارة هي طبقات تقوم بنفاذ الضوء بينما تعكس الحرارة في صورة الأشعة تحت الحمراء. في هذا البحث تم تحضير هذه المرايا كطبقتين: الأولى من الفضة و الثانية من أحد أكاسيد المعادن الانتقالية (أكاسيد المولبدينوم و الكروم و النيكل و الفاناديوم). الخصائص التركيبية تم دراستها بطريقة حيود الأشعة السينية ، و التي أوضحت أن طبقتي الفضة ¸ أكسيد النيكل فقط تلبورتا. الخصائص الطوبوغرافية لأسطح الطبقات تم دراستها بالمجهر الذري ، و الذي أوضح أن أسطح الطبقات تكونت من تشكيل عمودي. الخصائص الكيميائية لأكاسيد المعادن وتوزع العناصر في الطبقات المرايا تم دراستها بمطيافية الإلكترونات، و التي أظهرت انتشار العناصر في جميع الطبقات. :ذلك تم دراسة الخصائص الضوئية لأكاسيد المعادن (معامل الانكسار و طاقة الفجوة) و للمرايا (النفاذ و الانعكاس) و التي أوضحت أن الطبقات المصنعة تميزت بنفاذية عالية للضوء و انكاس عالي للأشعة تحت الحمراء.

CHAPTER 1: INTRODUCTION

1.1 Transparent Heat Mirrors

The solar spectrum consists of electromagnetic waves whose wavelengths (λ) extend from 200 nm to 3000 nm. The visible part of the spectrum extends from 400 to 700 nm, and corresponds to light. The upper wavelength part (700 to 3000 nm) corresponds to heat, that belong to infrared radiation. Conventional glass windows pass all parts of the solar radiation spectrum. Therefore, energy saving in buildings is based on enhancing the passage of the visible part while simultaneously suppressing the infrared part of the solar spectrum. To achieve these requirements, glass windows are coated with special types of thin films. Such coatings are therefore called spectrally-selective coatings. Metal /Dielectric multi-layer structures have been developed to achieve the desired requirements of transparency and heat reflection, and such a structure is thus called a transparent heat mirror (THM) [1].

Transparent heat mirrors are spectrally-selective energy efficient coatings that transmit the light and reflect the infrared (IR) heat. This subject has been extensively studied due to its wide range of energy saving applications. The THMs are classified into two basic categories. The first one is called cold THM, and is used in winter to reduce heating load. The cold THM, sometimes called black absorber, transmits both high energy solar radiation as well as near-infrared radiation inside the building. The infrared heat would be reflected back into the building. In this way, the majority of the solar energy can be utilized for day lighting and heating. The second type is called hot THM, and is used in hot climates to reduce the thermal /cooling load.

The hot THM allows the visible part of the solar spectrum to pass through windows and reflects the infrared part away from the building [2-4].

Transparent heat mirrors have been further divided into four types according to their layer structure. The first type is a thin metal film which should be thin enough to have high infrared (IR) reflectance and high visible transmittance due to low-enough visible absorption. The second type is a multilayer coating in which a thin metal film is coated by one or more anti-reflecting dielectric layers. The third type is either a single semiconducting film or a heavily doped semiconducting film which has sufficient wide band gap to afford transparency in the visible region and a high carrier concentration to obtain IR reflectance. The forth type is a conducting microgrid with appropriate controllable opening sizes that are large enough to transmit the visible radiation but sufficiently small compared to IR wavelengths so that the microgrid can work as an IR reflector [2,5-7]. In my work, I have used two layer metal /dielectric structure for fabrication of transparent heat mirrors. In which, silver was used as reflector and transition metal oxides were used to overcoat the silver to enhance the visible transmission and stability of THM.

The basic material used for thin-metallic film in THM is a metallic film which has high reflectance in the visible as well as in the infrared regions. All the metals have very high IR reflectance due to their high free-electron concentration. The noble metals Ag, Cu, and Au offer high infrared reflectance. High transparency in the visible range can be attained by minimizing the reflectance and absorption in the visible range. Very thin films are used to attain partial solar transparency. A very thin metal of 10-20 nm can be used as a heat mirror. It is reported that the

absorption coefficient of the films is equal to $4\pi\ k\ d/\lambda$ where k, d and λ are the extinction coefficient, film thickness, and wavelength respectively [8]. Thus, the absorption is reduced by decreasing the film thickness. The visible reflectance can be minimized by destructive interference between the beams reflected from the front and back of the metal film. Any discontinuity in the film affects the conductivity, and consequently it degrades the IR reflectance. Island formation is the main drawback of single metallic film that affects the IR reflectance more than the visible reflectance. This is because a discontinuous thin film not only loses conductivity but also IR reflectance as the electron gas is no longer free. The metallic layer behaves as an IR reflector and its reflectivity increases with thickness. The change in thickness of the metallic layer results in a greater change in the optical properties of the coating as compared to a change in dielectric thickness [9].

Silver is superior to other metals in THM applications because it has a plasma wavelength of about 320 nm and lowest visible absorption [10]. It has optical constants in the visible range (refractive index (n) = 0.06 and extinction coefficient (k) = 3.59 at λ = 550nm [11]) that suitably match the requirements of a THM.

Multilayer Transparent heat mirrors can be formed by sandwiching a thin metal film between two dielectric layers, this structure is known as a three-layer Dielectric/Metal/Dielectric (D/M/D) coating. The stability, durability and visible transmittance are significantly improved by over coating the dielectric on both sides of metallic thin film. The top layer of dielectric works as an anti-reflecting layer, which enhances the visible transmittance [12,13]. The best result for

transparent heat mirrors is obtained when the two dielectric layers on both side of metallic layer have the same thickness [14].

To incorporate and enhance the transmission in the visible range, the multilayer metal-dielectric coatings are used [10], where a dielectric acts as an antireflection coating on one side of the metal and increases the transmittance in the visible region [15]. These films are used to overcoat with a dielectric, metal oxide or semiconductor which essentially not only acts as antireflection coating and suppresses the visible reflectance but also enhance and improve the stability and durability of the THM [2]. Hence the visible transmittance, stability and durability of metal films are enhanced by overcoating the metal with a dielectric layer [15]. The selection criterion of the dielectric for a given metal is defined such that the refractive index (n) of the dielectric should be matched with extinction coefficient (k) of the metal in the desired range of the electromagnetic spectrum [9]. The dielectric layer, in a THM, serves three purposes. First, it works as an antireflection coating for the thin metallic layer, and therefore serves to increase the transmittance [15]. Second, it works as a protective coating for the underlying metallic layer [2]. Third, the thickness of the dielectric layer can tune the wavelength corresponding to maximum transmittance [16]. A dielectric with a high refractive index causes high reflectance in the IR range, while a dielectric with lower refractive index causes high transmission of light for the whole spectrum [17]. It has been revealed that the optimum performance of THM as D/M/D coating can be achieved when the refractive index of the dielectric layer (n_D) matches the extinction coefficient of the metal layer k_M. In this case, the greatest possible metal thickness occurs when the dielectric thickness is given by $d=\lambda/8n_D$ where λ is the wavelength at which THM is designed for maximum desired transmittance [15]. However, most dielectrics may have n_D less than k_M, and therefore the dielectric thickness may be greater than that given by $d=\lambda/8n_D$.

For a suitable transparent coating, the possible lowest value of the dielectric refractive index is approximately 1.96 [14]. In this work, transition metal oxides have been used as the dielectrics.

1.2 Transition Metal Oxides

Transitions metals oxides (TMO) have drawn immense interest over the last few decades due to their diverse and unique structural, chemical, optical, and magnetic properties that have rendered them crucial in several applied fields such as catalysis, optoelectronics, photovoltaics, protective coatings, and magnetism. The Transition metal oxides have attained a considerable attention for applications in the field of energy efficient coatings and energy efficient devices such as transparent heat mirrors, photochromic glasses, light sources, thermochromic windows, heat insulation of windows, solar collectors, electrochromic based windows and devices, and optical memory devices [17-22]. They are characterized by wide band gaps and relatively high refractive index and thus are suitable for THM applications. In this work; THM coatings were achieved by depositing a two-layer structure consisting of a transition metal oxide deposited on silver by thermal evaporation.

Selection criteria:

There are a large number of potential TMOs. Thus for THM fabrication, I have applied the following criteria to narrow down the selection of materials for my work:

1. Materials considered previously for THM applications have been excluded. This excludes TiO_2, HfO_2, and WO_3.
2. They should have a band gap less than 3.5 eV. Otherwise, they will transmit UV radiation. This excludes La_2O_3, Sc_2O_3, Ta_2O_5, Y_2O_3, and ZrO_2.
3. They should have a band gap larger than 2.5 eV. Otherwise, they will be colored and non-transparent in the visible. This excludes Co_3O_4, CuO, Fe_2O_3, and MnO_2.

4. Toxic materials should be excluded, since the intended application is for residential buildings. This excludes the oxides of mercury and cadmium.
5. They should be economically affordable. This excludes the noble metals and the rare earth metals.
6. They should be amenable to thermal evaporation. Sputtering is not suitable for these structures. This excludes the oxides of zinc and niobium.

These criteria left us with four TMOs, namely the oxides of chromium, molybdenum, nickel, and vanadium; and these are investigated in this work as the dielectrics for THM applications.

1.3 Literature Survey

Fan et *al.* [23] fabricated TiO_2/ Ag/TiO_2 films by rf magnetron sputtering. They were the first to use the concept of multilayer coating as a transparent heat mirror. These THM films have great potential for use as transparent thermal insulators and in solar-thermal power conversion due to apparent stability and their excellent optical properties. They observed that the fabricated transparent heat mirrors had 98-99% infrared reflectivity and 84% visible transmission. These heat mirrors appear to have good thermal and chemical stability.

Karlsson et *al*. [5] studied the influence of using numerous noble metals with ZnS as the dielectric. They deduced that silver is the best choice for transmission filters in optical and solar energy applications. However, gold is equally good, or even a better candidate for a situation where a broad band transmission is required. Karlsson et *al*. [5] also studied the properties of single semiconducting films of SnO_2, single semiconducting films of ZnS and triple layer of

SnO_2/metal/SnO_2, and ZnS/metal/ZnS. They concluded that solar heating of single SnO_2 and triple layer coatings had equal values but their thermal insulation is greater than that of a single layer.

Hasan et *al*. [7] investigated single and multilayer films based on TiO_2 and Ag using rf magnetron sputtering. Single layer TiO_2 films exhibited a high transmittance of order 80% in the visible region and high refractive index of order 2.31 at a wavelength of 550 nm. Single layer Ag films of nanometer thickness (18 nm) exhibited very low transmittance (below 10%) in the infrared region with a moderate transmittance in the visible region. A bi-layer TiO_2/Ag film showed limited heat-mirror effect with a visible transmittance of about 40% and low infrared transmittance (about 25% at 2500 nm). However, for the multilayer film of TiO_2/Ag/TiO_2, high infrared transmittance was observed.

Kostlin et *al.* [15] prepared ZnS/Ag/ZnS based THMs by thermal evaporation. The thickness of the central silver layer was varied between 3 to 40 nm. The thickness of the second layer of ZnS film was varied to get optimum visual transmittance while keeping the first layer of ZnS constant to 30 nm. The experimental results of spectral transmission and reflection revealed that too thin a silver film was not a good infrared reflector but it became more or less absorbing whereas too thick a silver film was good reflector even in the visible range. They concluded that with an optimum silver thickness, high visual transmittance and high IR reflectivity can be achieved.

Leftheriotis et *al*. [14] deposited the three layer structure (dielectric/metal/dielectric) ZnS/Ag/ZnS THM by thermal evaporation. They determined the optical properties of single

layer Ag deposited on glass for different thicknesses ranging from 16.5 to 26 nm. They observed that with increase in the thickness, transmission decreased and the film showed increasingly improved mirror-like behaviour. The optical properties of ZnS/Ag/ZnS multilayered THM were measured after each layer deposition in order to investigate the existence of a process that may cause film slow degradation. It was found experimentally that ZnS not only act as an antireflection coating to the metallic (Ag) layer, but also to stabilize the mirror (ZnS/Ag/ZnS film) in order to avoid further degradation, enhance its adherence and improve the thermal resistance of film up to 240°C.

Al-Kuhaili [24] used electron beam evaporation to deposit thin films of hafnium oxide. The optical measurement revealed that hafnium oxide thin films were relatively dense, and possessed a relatively high refractive index as well as high transparency up to 300 nm. In addition to these optical properties, the mechanical, chemical and thermal stability of the thin film enable hafnium oxide to be a suitable candidate for use in energy saving applications.

Al-Kuhaili et *al.* [10] used the three layer structure to fabricate transparent heat mirrors based on tungsten oxide/silver thin films using thermal evaporation. The energy efficient coatings based on WO_3/Ag/WO_3 thin films acquired all the desired properties of THMs. They observed a maximum transmittance of 88.3% at 554 nm, which was amongst the highest reported value for THMs based on metal-dielectric coatings. They deduced that tungsten oxide is not only a suitable material for use as the dielectric in THMs but also it is one of the best dielectrics for such applications.

Al-Kuhaili et *al.* [25] fabricated transparent heat mirrors based on multilayers of gold and tungsten oxide by thermal evaporation. They studied the optical properties of WO_3/Au/WO_3 THMs as a function of the thickness of gold, where the thickness of the gold layer was varied for a fixed WO_3 thickness. They observed that the transmittance decreases as the thickness increased, with a complementary improvement of infrared reflectance.

Durrani et al. [26] designed energy-efficient coatings for warm climates using a three-layer structure (dielectric/metal/dielectric) on a glass substrate. A thin silver layer was used as a metallic layer sandwiched between two dielectric layers such as WO_3, ZnS, and TiO_2 by thermal evaporation. They concluded that the transparent heat mirror with any of the three dielectrics was highly energy-efficient and the efficiencies of these THMs with different dielectrics were almost the same. Temperature measurements revealed a difference of about 8 ^oC with and without coated windows.

A number of workers have used semiconductor metal oxide single thin films as THMs. [3,19,27-35]. Such single semiconducting films include the doped and undoped SnO_2, In_2O_3, ZnO, and Cd_2SnO_4 with suitable carrier concentrations. The visible transmission, IR reflection and the associated cut-off wavelength are the most important properties that are desired for a mirror. All values were interrelated to the film density, thickness, and mobility of the free electrons in the film and can be calculated for a given material using the interference equations and the optical constants associated with refraction and absorption respectively [29]. These metallic oxide and semiconducting films had very favorable properties for THM applications. The band gap of an undoped transition metal oxide is about 3 eV. Proper doping is required to

achieve a band gap that is suitable for high infrared reflection without affecting the transmittance adversely in the visible region. In order to have low emissivity, the sheet resistance of the fabricated film should be less than 20 Ωcm^{-1}.

Dewaal et *al.* [36] investigated that for an optimum transparent heat mirror based on SnO_2, a high electron mobility of at least 4.0 $cm^2V^{-1}s^{-1}$ and a free electron concentration of about 3×10^{20} cm^{-3} are required. The tin-doped indium oxide became more favorable than SnO_2 films due to high conductivity and infrared reflection as the consequence of greater free charge carrier density. Moreover, higher reflectance was observed in tin-doped indium oxide due to higher electron mobility.

1.4 Scope of Work

Transparent heat mirrors (THM) allow the visible range of electromagnetic radiation to be transmitted through them but reflect the infrared part. In order to realize this potential, in this work, the two layer dielectric/metal system (D/M) was used to fabricate THMs on different types of substrates by using thermal evaporation. The D/M multilayers were deposited using different transitions metal oxides (TMOs) as dielectrics.

In this work, I used thermal evaporation to fabricate THMs based on the transition metal oxides Cr_2O_3, MoO_3, NiO, and V_2O_5. This technique was selected because of several attractive features:

1. Simplicity of deposition
2. Ultraclean deposition, and thus less contamination
3. Superiority for multilayer growth
4. The grown films have superior optical and morphological features

I first deposited individual oxide layers and investigated their properties that are of relevance to THMs. Then, I fabricated THMs and investigated their properties. In addition, I evaluated the performance of these mirrors as required for energy-saving applications.

MoO_3 and V_2O_5 were deposited by thermal evaporation from resistively-heated boats, whereas NiO and Cr_2O_3 were fabricated by electron-beam (e-beam) evaporation. The selection of either technique is material-dependent.

Specifically, the work progressed as follows:

1. Deposit NiO thin films by electron-beam evaporation.
2. Characterize the properties of NiO thin films.
3. Deposit a two layer structure THM NiO/Ag, using e-beam evaporation for NiO and thermal evaporation for Ag.
4. Characterize the properties of the THM.

This procedure was repeated for the other three oxides.

The structural properties of the films were studied using X-ray diffraction and atomic force microscopy techniques.

The chemical properties of the films were characterized by X-ray photoelectron spectroscopy. Depth profiling was employed to investigate the properties of the mirrors.

The optical properties were determined through spectrophotometry.

CHAPTER 2: Experimental Techniques and Characterization

2.1 Thermal evaporation

There are several techniques to deposit thin films. Thermal evaporation is one of the most suitable and extensively used techniques for the growth of THM thin films. The basic idea of this technique is to evaporate the target (powder or pellets) in high vacuum (typically of the order of 10^{-5} mbar) to deposit the thin films. A schematic diagram of a thermal evaporation system is shown in Figure 2.1. A resistively heated tungsten or molybdenum boat was used to evaporate the materials.

Electron beam evaporation is one of the extensively used techniques for thin film fabrication. A schematic diagram representing electron beam evaporation is shown in Figure 2.2. An intense beam of high energy electrons is used to vaporize the material placed in a crucible which cannot be vaporized with heated source [37-39]. A heated filament is used as electron source which emits the electron beam thermionically. An electric field is used to accelerate the electron beam which is further focused by electric and magnetic fields on the evaporant in the crucible. The kinetic energy of electrons is converted into thermal energy in the form of heat after interaction with evaporant material. This phenomenon leads to evaporation of material and the vapor flow is used to deposit the thin films on substrates.

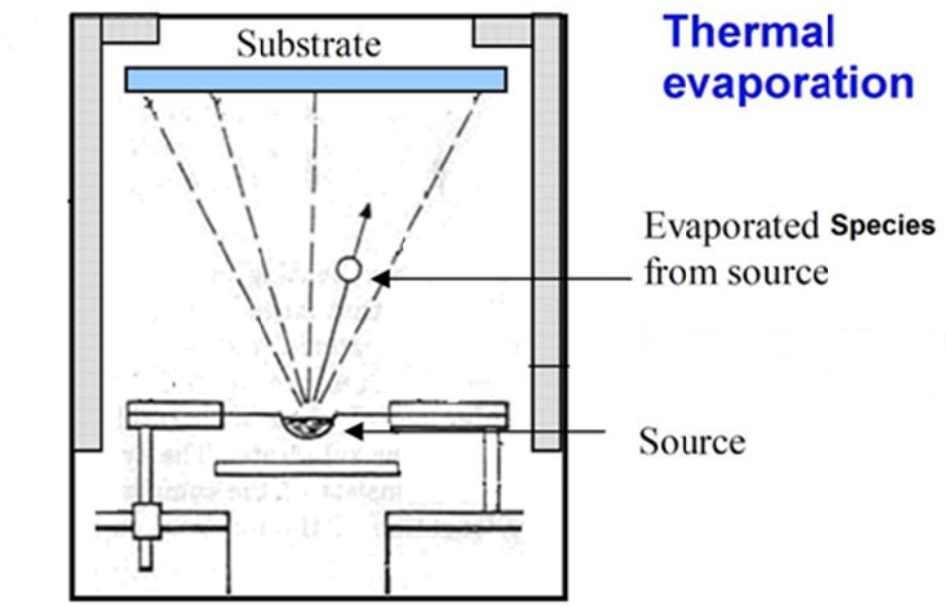

Figure 2.1 Schematic diagram of thermal evaporation.

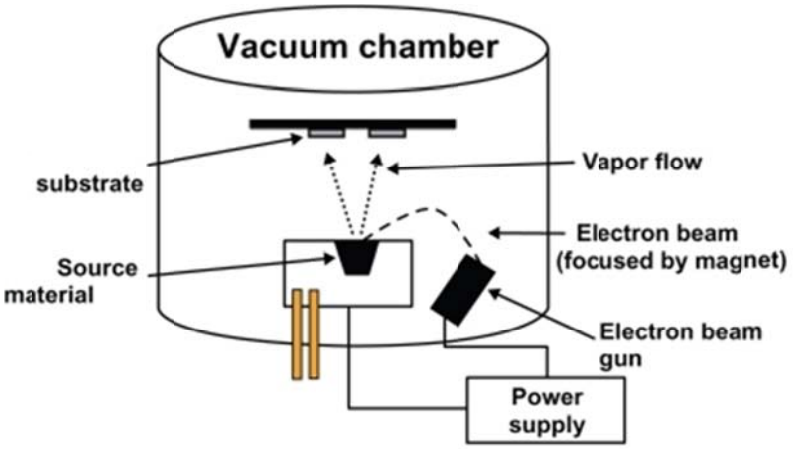

Figure 2.2 Schematic diagram of e-beam evaporation.

2.2 Characterization Techniques

After deposition, samples were removed from the deposition chamber and several characterization techniques were applied to study the surface morphology, chemical composition, structural, and optical properties.

2.2.1 X-ray diffraction

X-ray diffraction (XRD) is an important method used to study and characterize the structure, preferred orientation, stress, strain and crystallite size in solid samples. It works on the principle of Bragg's law. A monochromatic X-ray beam of wavelength λ is used as probe, which is projected on the surface of crystal at an angle θ. The incident x-rays undergo diffraction from successive planes of the crystal. The distance travelled by the diffracted rays must be an integral multiple *m* of wavelength in order to satisfy Bragg's condition [40].

$$m\,\lambda = 2\,a\,\sin\theta \qquad (2.1)$$

where *a* is the lattice spacing between the planes of the crystalline material. The schematic diagram of XRD mechanism is shown in Figure 2.3. Two phenomena occur during X-ray diffraction from planes of crystal; constructive interference and destructive interference. The constructive inference appears as peaks correspond to each plane of the crystal in the XRD spectrum, which represents the distribution of atoms in material. A solid state detector is used to detect these diffracted X-rays. The data is further processed by electronic circuit and identified in computer. This processed data is finally used to identify the material and calculate the elemental concentration in compound.

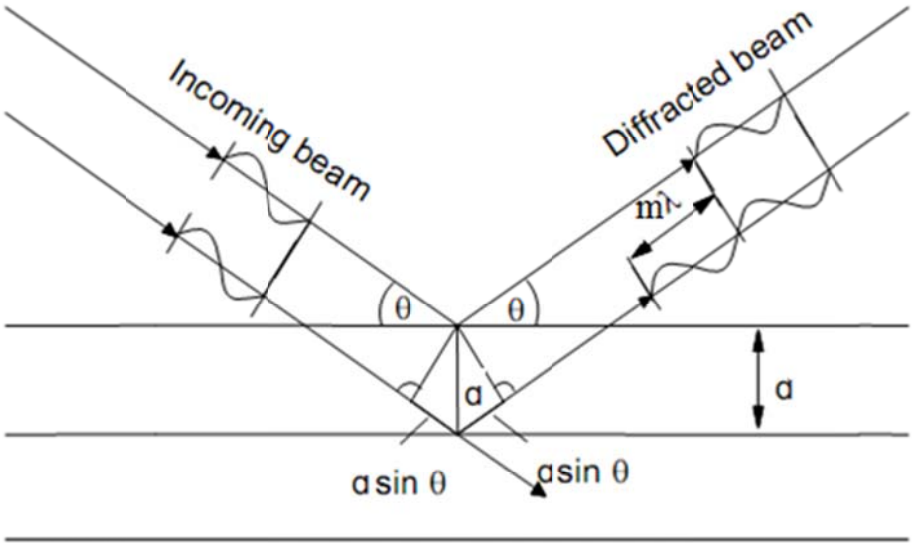

Figure 2.3 Schematic diagram of X-ray diffraction representative of Bragg's law.

2.2.2 Atomic force microscopy

Atomic force microscopy (AFM) is a surface characterization technique used to study the surface morphology of materials and thin films. The surface resolution of AFM is order of fraction of a nanometer. AFM employs a cantilever to scan the surface of a material, which has a very sharp tip of the order of few nanometers. To measure the surface roughness, the tip is brought very close to surface. The forces between surface and tip are measured by deflection of the cantilever through a deflection sensor. These forces are mechanical contact forces, bonding forces, van der Waals forces, capillary forces, magnetic forces, electrostatic forces, salvation forces, and Casimir forces. An electronic system, equipped with laser and array of photodiodes, is used to measure the deflection of the cantilever. The deflected laser spot form the head of the cantilever is

detected by photodiode sensors. A feedback mechanism is used to keep the deflection constant by adjusting the distance between the cantilever tip and sample surface, which maintains a constant force between them [41]. Figure 2.4 shows a schematic diagram of an AFM.

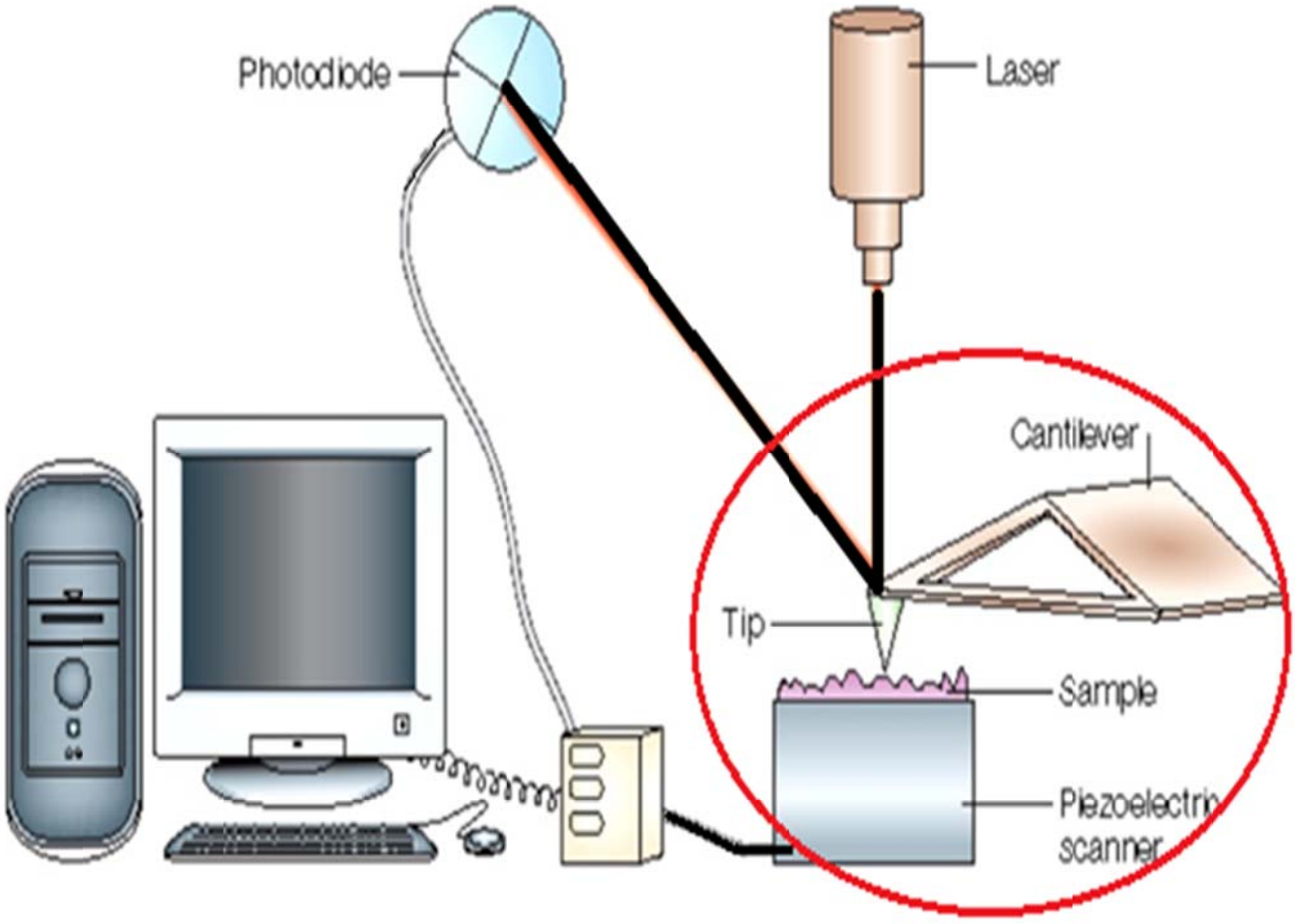

Figure 2.4 Schematic diagram of the working principle of an atomic force microscope.

2.2.3 X-ray photoelectron spectroscopy

X-ray photoelectron spectroscopy (XPS) is a surface and chemical analysis technique, in which the sample is exposed to an incident soft X-ray beam and the kinetic energies (E_k) of the ejected photoelectrons are measured. XPS works on the principle of the photoelectric effect, in which the binding energy of the core electrons is overcome by the incident X-ray beam energy as shown in Figure 2.5. When the electron binding energy of a core electron is overcome by the X-ray beam, the electron is ejected from the material and the kinetic energies of the ejected electrons (E_k) is measured by using an electron spectrometer [42,43]. The work function of the electron spectrometer is ϕ. By using the law of conservation of energy, the binding energy (E_B) of the ejected electrons are calculated.

$$hV = E_B + E_k + \phi \quad (2.2)$$

$$E_B = hV - (E_k + \phi) \quad (2.3)$$

The hV is energy of an incident X-ray photon, where h is plank constant and V is frequency of photon. The binding energy of an ejected photoelectron is characteristic of the orbital from which the electrons were ejected. Hence each element in the periodic table has some specific or characteristic binding energies that are signatures of that element. The XPS technique can identify the entire periodic table elements except hydrogen (H) and helium (He) [42-44].

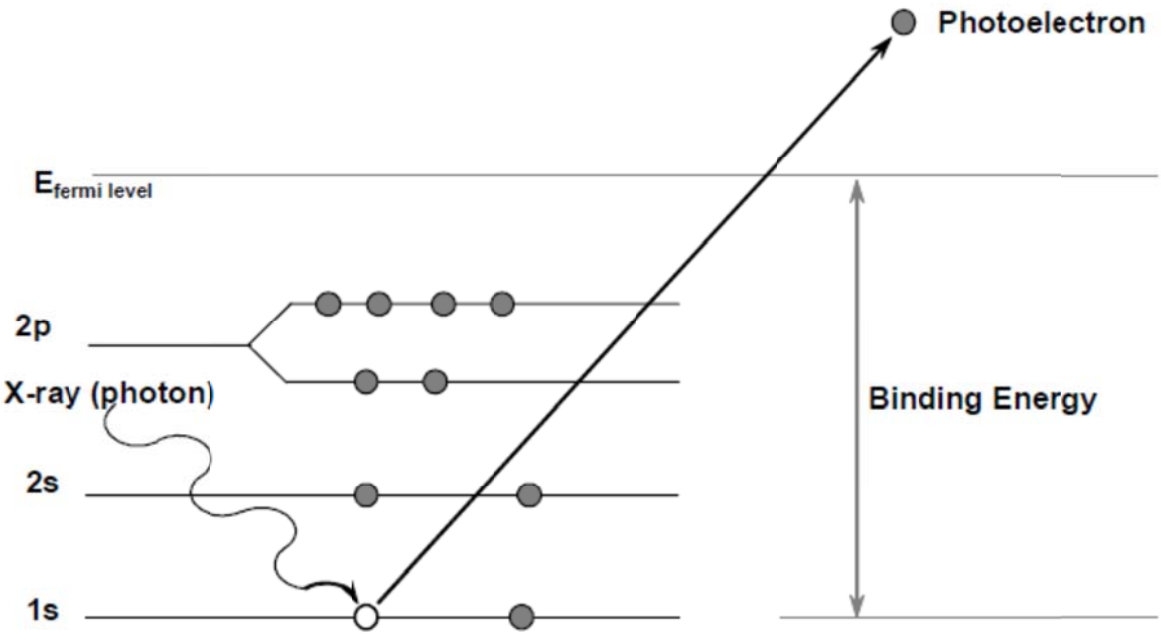

Figure 2.5 Schematic diagram of the basic principle used in XPS.

2.2.4 Spectrophotometry

The optical properties (transmittance and reflectance) of the single oxide thin films and transparent heat mirrors were measured by a double beam uv-spectrophotometer. By plotting these optical measurements as function of wavelength, we can calculate the absorption coefficient, band gap, refractive index, extinction coefficient and integrated spectral quantities (integrated visible transmittance and integrated infrared reflectance). The interaction of incident light with a thin film is explained in Figure 2.6. When electromagnetic radiation interacts with a transparent thin film, part of it is reflected from the front surface and a fraction of is transmitted through the film. Another part of light is absorbed as well as scattered by surface and volume imperfections.

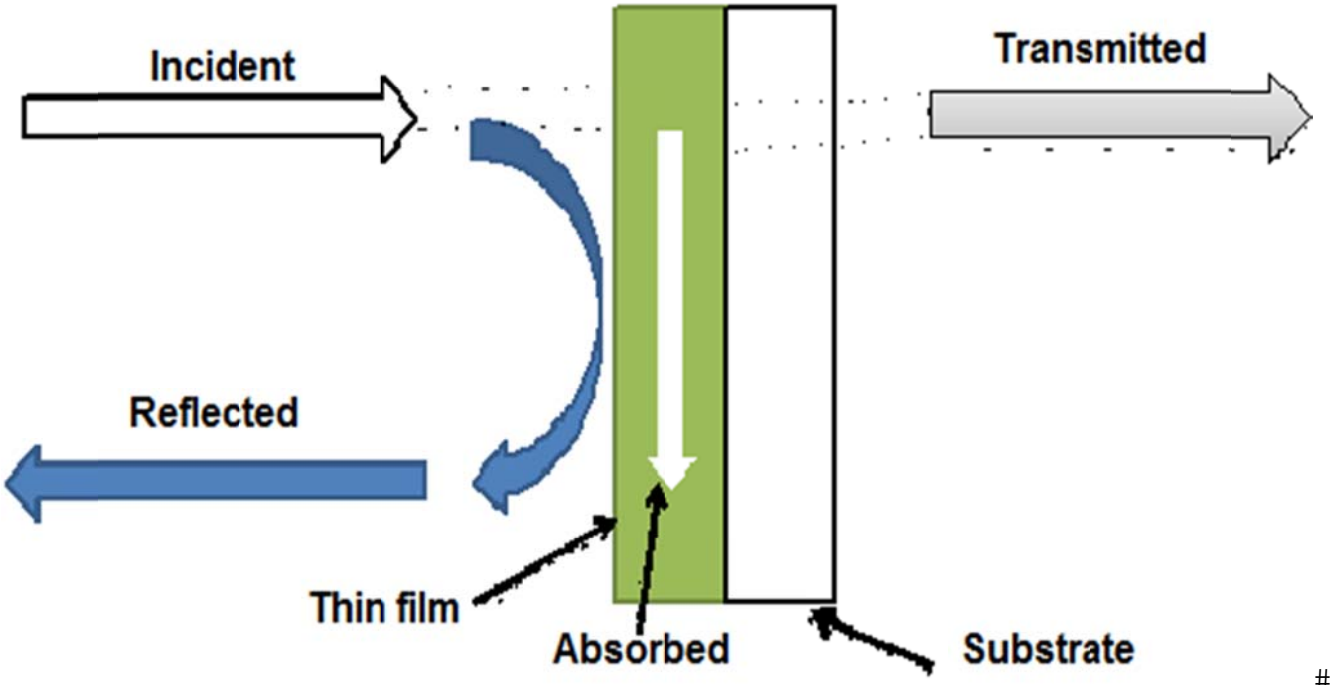

#

Figure 2.6 Basic principle of optical measurements of a thin film.

A Double beam spectrophotometer is an instrument used to measure the intensity of reflected or transmitted light as a function of wavelength. It compares the light intensity coming from two different sources, one source containing the reference beam and the other coming from or through specimen. A schematic diagram explaining the working mechanism of double beam spectrometer is shown in Figure 2.7.

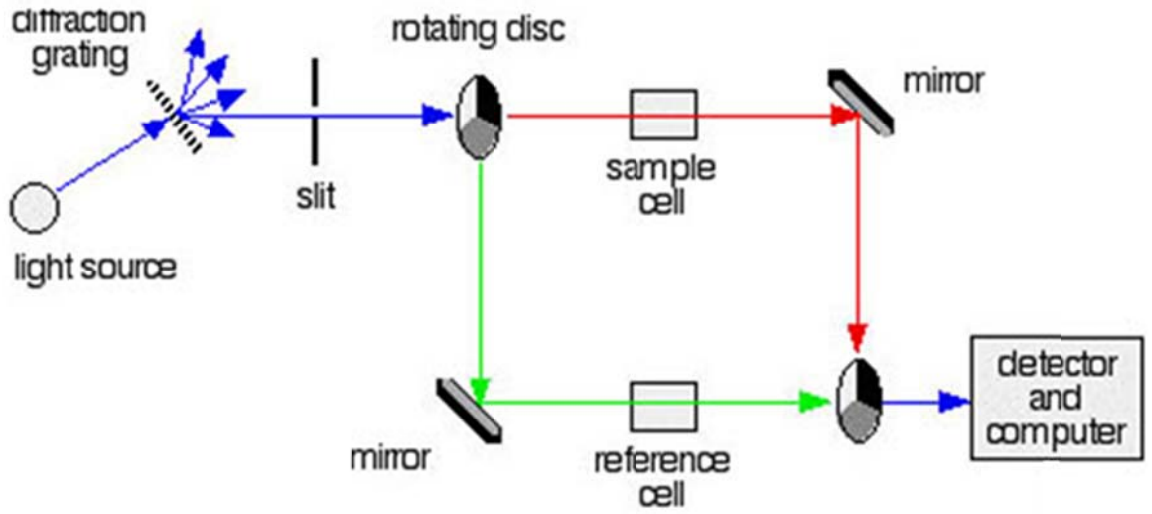

Figure 2.7 Schematic diagram of a double beam spectrophotometer.

2.3 Sample preparation and characterization

In my work, the thin films were fabricated in a Leybold L560 box coater, which is pumped by a turbo-molecular pump (Figure 2.8). The system was pumped down to a base pressure (initial pressure) of 4×10^{-5} mbar. The starting materials were slowly outgassed before evaporation. The films were simultaneously deposited on fused silica and tantalum substrates in order to use them for different characterizations. The substrates holder was rotated during the deposition for uniform smooth films, and kept unheated. A quartz crystal thickness monitor and rate controller were used to monitor and control the film thickness and evaporation rate, respectively. The film thickness was determined optically, as will be discussed in chapter 3. In order to fabricate THM the thin silver film deposited on glass substrate was overcoated by TMO. The thickness of TMOs was controlled for optimum performance of transparent heat mirrors such that the refractive

index of TMOs matched with extinction coefficient of silver. The parameters pertinent to each material are shown in Table 2.1.

Figure 2.8 Leybold L560 box coater.

Traditionally, THMs have been fabricated using the three-layer dielectric/metal/dielectric multilayer coatings. In this work, I used a two-layer TMO/Ag structure as a THM. This simpler structure provides ease of fabrication, saving of materials (and thus economic value), and less parameters to be optimized. For the two-layer structure, the layers were deposited without breaking the vacuum, and with the silver film first deposited on the substrates. The silver powder (99.999% purity) was evaporated from a molybdenum boat, with an evaporation rate of 0.1 nm/s. The thickness of the silver layer used with each oxide was: 20 nm, 40 nm, 20 nm, and 40 nm for Cr_2O_3, MoO_3, NiO, and V_2O_5, respectively.

A number of characterization techniques have been taken up to examine the properties of the films. X-ray diffraction was employed to investigate the structural properties of the thin films, which was performed in a RigakuUltima IV diffractometer using Cu K_α radiation. The

parameter setting of XRD comprises of 2θ step and the step acquisition time kept at 0.02^{o} and 1.00 s respectively. The chemical composition of the TMO films and two layer structures was investigated using X-ray photoelectron spectroscopy (XPS). The experiment was performed in a Thermos Scientific Escalab 250Xi spectrometer equipped with a monochromatic Al K_{α} (1486.6 eV) x-ray source. The resolution of the instrument was 0.5 eV. During the XPS characterization, the specimen chamber was kept at ambient temperature and at a pressure of 5×10^{-10} mbar. The spectra were referenced with adventitious C 1s peak at 284.5 eV. The films deposited on tantalum substrates were used for the XPS analysis, so that surface charging of non-conducting samples could be reduced. The error in measured binding energy values by XPS was about 0.2 eV. Elemental depth profiles of the films in the multilayer structure were performed to study the spatial distribution of elements. XPS measurement was obtained successively after 20 second ion-etching. Etching was performed using a 2-keVAr^{+} ion beam on a 1 mm^2 area of the surface. During depth profile analysis, the chamber was maintained at pressure of order 3×10^{-8} mbar, and the ion current at the sample surface was less than 1 μA.

The surface morphology of the thin films was studied by using contact mode atomic force microscopy (AFM) (Veeco Innova diSPM). The scanned surface area was 2×2 μm^2, and the constant scan rate was 2 Hz. A silicon tip of radius 10 nm, which is oscillating at its resonant frequency of 300 kHz was used to probe the specimen surface. The optical properties of the individual thin films and transparent heat mirrors were determined by measuring the normal-incidence transmittance (T) of the films over the electromagnetic spectrum range of 200–800 nm, using a Jasco V-570 spectrophotometer. Normal-incidence reflectance (R) and transmittance spectra of the heat mirrors were measured over the spectral range of 200–2000 nm.

Table 2.1 Designed parameters used for thickness of single and bi-layer films

Material	Starting Material	Purity	Evaporation rate (nm/s)	Evaporation Method	Single-film Thickness (nm)	Multilayer Thickness (nm)	Oxygen Partial pressure (mbar)
MoO_3	MoO_3 powder	(99.5%)	0.2	Mo boat	177	40	---
Cr_2O_3	Cr_2O_3 pellets	(99.9%)	0.1	e-beam	158	40	5×10^{-4}
V_2O_5	V_2O_5 powder	(99.995%)	0.1	W boat	140	40	---
NiO	Ni pellets	(99.99%)	0.1	e-beam	120	30	5×10^{-4}
Ag	Ag powder	(99.999%)	0.1	Mo boat	20-40 nm	depends on oxide	---

CHAPTER 3: NICKLE OXIDE THIN FILMS

3.1 Introduction

Nickel oxide (NiO) is a wide band gap semiconductor that is characterized by excellent stability, switchable electrical and optical properties, and p-type conductivity. NiO thin films have been investigated in potential applications, such as electrochromic coatings [45], resistance switching [46], gas sensing [47], p-type transparent conductors [48,49], and organic photovoltaics [50,51]. Several techniques have been used for the synthesis of NiO thin films, including sputtering [46-49,52-54], chemical solution deposition [50,51], chemical vapor deposition [55], atomic layer deposition [56], and thermal evaporation [57,58]. Nickel oxide/metal multilayer structures have been used in a variety of spectrally-selective solar applications. For example, NiO/Ni thin films have been used as selective solar absorbers [59].

3.2 Properties of Nickel Oxide Thin Films

In this work, nickel oxide thin films were deposited by the reactive electron-beam evaporation of pure nickel pellets under an oxygen partial pressure of 5×10^{-4} mbar.

3.2.1 Structural Properties

The structural properties of the films were investigated through XRD and AFM. A typical XRD pattern of a nickel oxide thin film is shown in Figure 3.1(a). Classification of the materials, and

peak identification were based on data from the International Center for Diffraction Data (ICDD) [60]. The films showed preferential growth along the (200) direction of cubic NiO. Figure 3.1(b) shows the XRD pattern of the transparent heat mirror (NiO/Ag), which exhibits the (111) peak of silver in addition to the NiO(200) peak. In both cases, there was no indication of the presence of metallic nickel, within the detection limits of XRD.

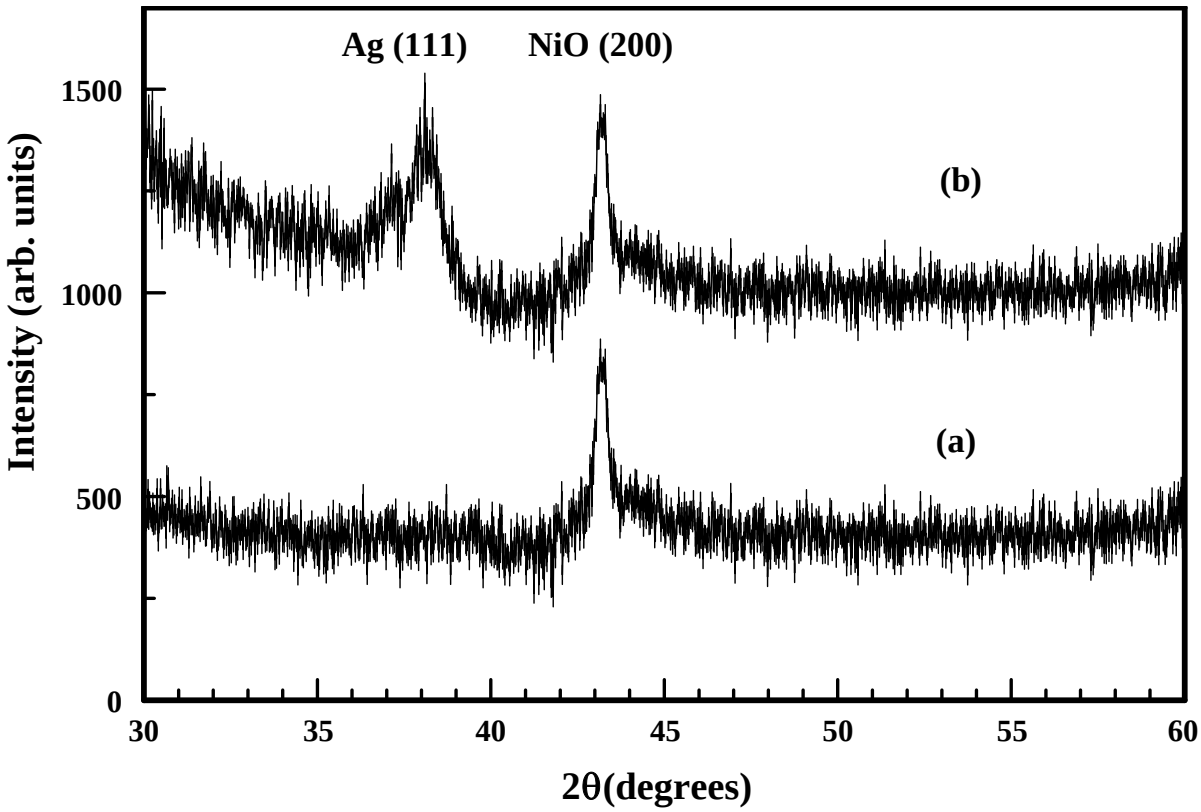

Figure 3.1 XRD spectra: (a) A nickel oxide film, (b) A transparent heat mirror (consisting of a nickel oxide layer on top of a silver layer).

Figures 3.2 (a and b) show characteristic three-dimensional AFM images of individual nickel oxide and silver thin films, respectively. The surfaces exhibited a columnar structure. The root mean square surface roughness (R_{rms}) of the nickel oxide films was 0.52 nm, indicating a smooth surface. The R_{rms} value for the silver films was 2.80 nm, indicating a rough and porous structure.

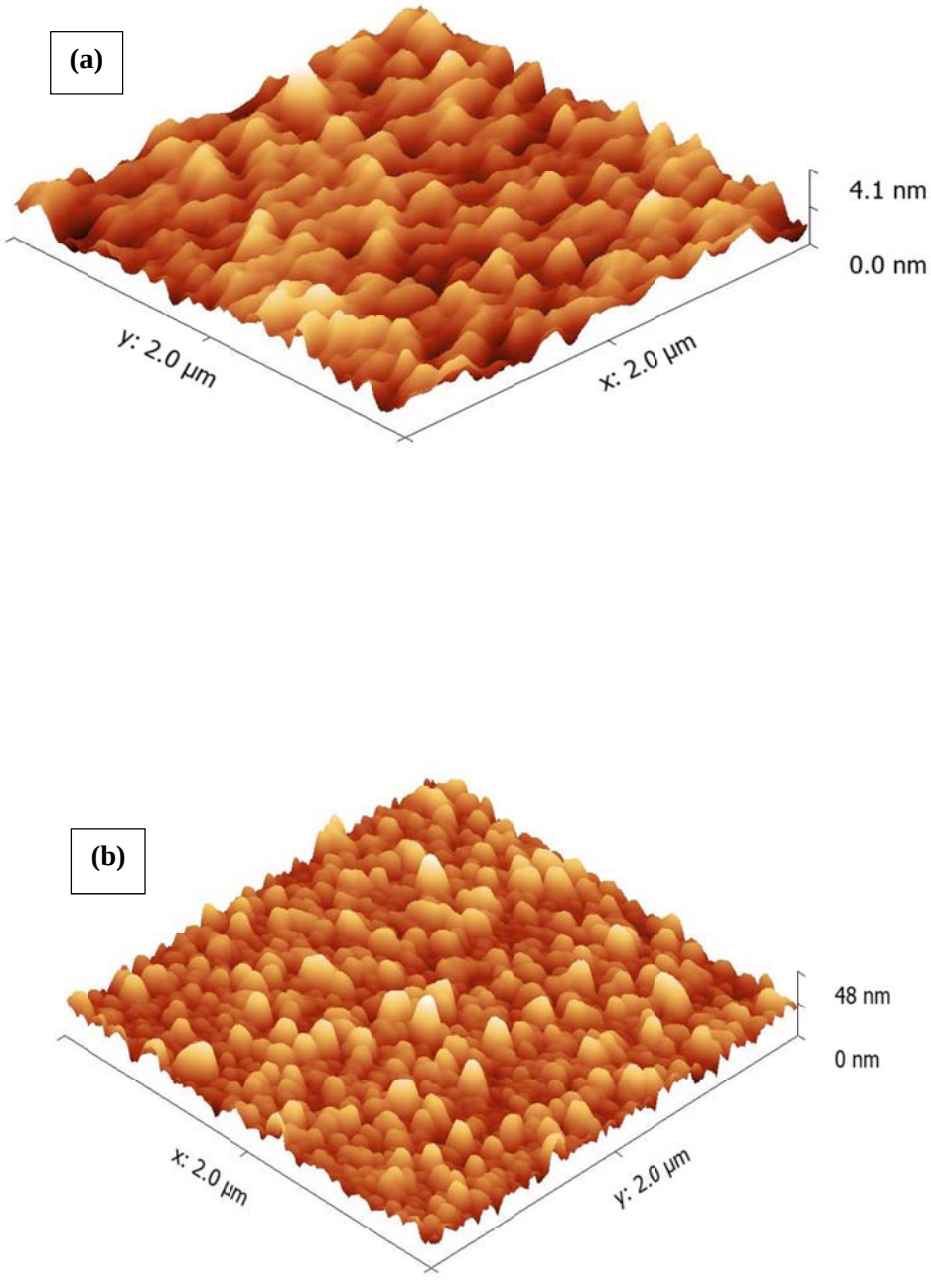

Figure 3.2 Three dimensional AFM micrographs: (a) nickel oxide thin film with a thickness of 120 nm, (b) silver thin film with a thickness of 20 nm.

3.2.2 Chemical Properties

The chemical state and composition of the films were investigated using XPS. This technique is sensitive to core level shifts and is able to give information on the metallic environment and oxidation state [61]. The nickel XPS 2p core level spectrum consists of two sublevels ($2p_{1/2}$ and $2p_{3/2}$) due to spin-orbit splitting. The Ni $2p_{3/2}$ spectrum is very complex due to the existence of several oxidation states, including Ni^{2+} (NiO and $Ni(OH)_2$) and Ni^{3+} (Ni_2O_3). Moreover, each oxidation state is accompanied by major and minor peaks, as well as satellite peaks [52,55]. In addition, the different oxidation states overlap, which complicates the assignment of a certain peak to an oxidation state [45]. There is a significant variation and overlap in the reported values of the binding energies (BE) of the different oxidation states of nickel in the $2p_{3/2}$ core level region [45,47,48,51-53,55,57]. This wide spread of values, along with conflicting assignments, arise not only from the inherent overlap of the oxidation states but also from the experimental parameters. Most assignments of binding energies were based on the C ls peak, whose values could differ by as much as 1 eV from one investigator to another. Also, some papers reported etching of the sample surface by ion bombardment prior to XPS analysis, which causes shifts in the binding energy values [52].

XPS spectra of my NiO thin films were obtained in the Ni $2p_{3/2}$ and O1s core level regions, and are shown in Figure 3.3. In order to find out the binding energies in the Ni $2p_{3/2}$ region, the spectrum was deconvoluted using a non-linear least squares algorithm with a Shirley background and a Gaussian—Lorentzian mixed line shape. The resolution of the Ni $2p_{3/2}$ spectrum into its component peaks is shown in Figure 3.3(a). The binding energies weights, and assignments of these components are given in Table 3.1. The weight of a component can be

calculated by dividing its area by the total area of the Ni $2p_{3/2}$ spectrum. The assignments were based on data from references [45,48,51,57]. The first two components (A and B) were assigned to NiO. They may arise from multiplet splitting in NiO [52,55]. Components C and D may be assigned to $Ni(OH)_2$ and Ni_2O_3, respectively. They arise from the exposure of the films to air [62]. The O1s spectrum was resolved into two components (A and B), as shown in Figure 3.3(b). The binding energies, weights, and assignments of these two components are given in Table 3.1. The assignments were based on the binding energy values given in references [45,62]. The O 1s high binding- energy component (B) may be assigned to Ni_2O_3, $Ni(OH)_2$, and adsorbed oxygen species (such as water and carbonates) that result from exposure of the films to air.

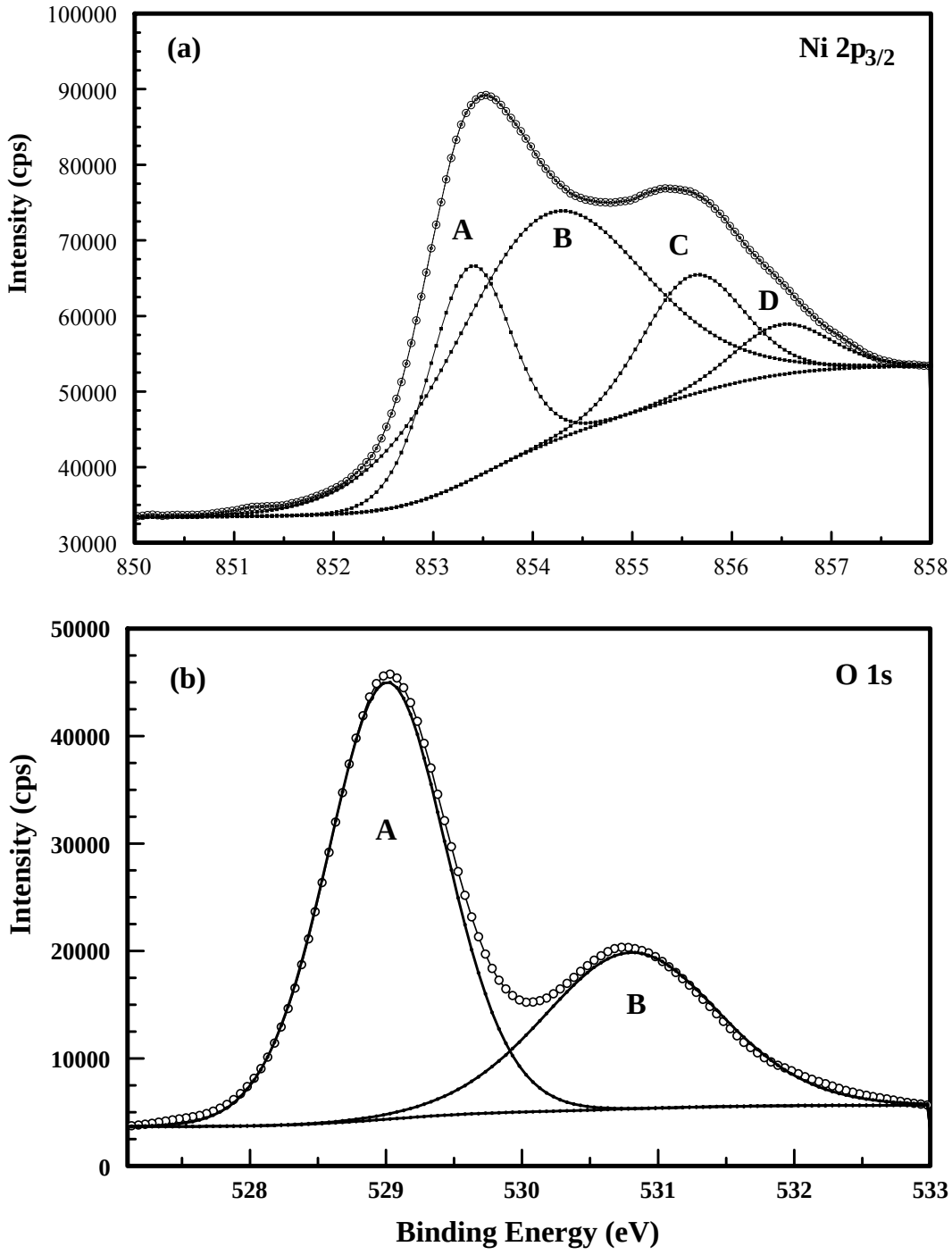

Figure 3.3 XPS spectra of nickel oxide thin films: **(a)** Ni $2p_{3/2}$ core level spectrum, **(b)** O1s core level spectrum. The experimental spectra are represented by the open circles. The spectra were deconvoluted into their component peaks.

Table3.1 Summary of the resolved components of the Ni 2P3/2 and O 1s spectra.

Peak	Component	BE (eV)	Γ (eV)	%W	Assignment
Ni $2p_{3/2}$	A	853.37	0.96	22.2	NiO
	B	854.15	2.26	56.23	NiO
	C	855.60	1.2	15.42	$Ni(OH)_2$
	D	856.50	1.13	6.15	Ni_2O_3
O 1s	A	529.01	1.04	65.67	NiO
	B	530.80	1.52	34.33	

B.E=Binding Energy, Γ=Full width at half maximum, W=Weight of the component

3.2.3 Optical Properties

The normal-incidence transmittance spectrum of a nickel oxide film is shown in Figure 3.4(a). This spectrum was used to calculate the optical constants of the film. In the transparency region of the film (λ > 400 nm), the transmittance spectrum was fitted with the equation of the transmittance for a thin film on a transparent substrate [63,64]:

$$T = \frac{16n_s(n^2+k^2)\beta}{A+B\beta^2+2\beta[C\cos(4\pi nd/\lambda)+D\sin(4\pi nd/\lambda)]} \tag{3.1}$$

With

$$A=[(n+1)^2+k^2][(n+n_s)+k^2]$$
$$B=[(n-1)^2+k^2][(n-n_s)+k^2]$$
$$C=-(n^2-1+k^2)(n^2-n_s^2+k^2)+4k^2n_s$$
$$D=2kn_s(n^2-1+k^2)+2k(n^2-n_s^2+k^2)$$

where *n, k* and *d* are refractive index, extinction coefficient, and thickness of the film, respectively and n_s is refractive index of the substrate, and $\beta = exp(-4\pi kd/\lambda)$. Dispersion models of *n* and *k* must be implemented in order to use equation (3.1) to fit the experimental transmittance spectra. Cauchy dispersion equation was employed to model the refractive index:

$$n(\lambda) = n_o + \frac{A_1}{\lambda^2} + \frac{A_2}{\lambda^4} \qquad (3.2)$$

where n_0, A_1, and A_2 are constants. The extinction coefficient *k* was modeled by constant absorption (k_0) in addition to scattering:

$$k(\lambda) = k_o + \frac{B}{\lambda^3} \qquad (3.3)$$

where *B* is a constant. The experimental transmittance spectrum was fitted using equation (3.1), with equations (3.2) and (3.3) as the models for the optical constants. The fitting parameters were n_o, A_1, A_2, k_o, *B*, and *d*. There was an excellent fit of the experimental spectrum by the theoretical model, with a correlation of at least 99.5 %. The best-fit parameters were $n_o = 1.97$, $A_1 = 3.41 \times 10^4$ nm^2, $A_2 = 3.74 \times 10^8$ nm^4, $k_o = 6.03 \times 10^{-3}$, $B = 1.09 \times 10^6$ nm^3, and $d = 120$ nm. These parameters were used to calculate the refractive index and extinction coefficients of the films, whose dispersion curves are shown in Figure 3.4(b). My values of the optical constants are in close agreement with those reported in the literature [64].

No comparison of my values of the optical constants with previous reports can be made, since these constants depend critically on the deposition technique and the preparation conditions, and therefore their values vary significantly from one report to another. However, my values of the refractive index may be compared with the bulk value to estimate the relative density of the nickel oxide films. Lorentz-Lorenz relation was used to estimate the density of the film [16]:

$$\frac{\rho_f}{\rho_b} = \frac{(n^2-1)(n_b^2+2)}{(n^2+1)(n_b^2-1)} \quad (3.4)$$

where ρ_f is the density of the film, ρ_b is the density of the relevant bulk material, and n_b is the bulk refractive index whose value is 2.182 at λ = 550 nm [65]. Using n = 2.089 at λ= 550 nm (Fig. 3.4b), the relative density (ρ_f/ρ_b) was 0.95.

In the fundamental absorption region, the absorption coefficient (α) may be calculated from the transmittance using the approximate relation:

$$\alpha = \frac{1}{d}\ln(\frac{1}{T}) \quad (3.5)$$

The absorption coefficient α was calculated using Eq. (3.5), and its variation as a function of photon energy (E) is shown in Fig. 3.4 (c). Above the fundamental absorption edge, the relationship between the absorption coefficient of a semiconductor material and the incident photon energy can be written as:

$$\alpha E = \alpha_o (E - E_g)^{\eta} \quad (3.6)$$

where α_o is a constant, and E_g is the band gap of the material. The exponent η depends on the type of transitions involved, as follows: η = 1/2 consistent to a direct allowed transition whereas η = 2 relates to an indirect allowed transition. To obtain the band gap, $(\alpha E)^{1/\eta}$ was plotted as a function of photon energy, and such type of plot is called a Tauc plot. The best fit to my films was obtained with η = 1/2. A plot of $(\alpha E)^2$ as a function of photon energy is shown in Fig. 3.4(c). The linear portion of the curve was fitted using linear regression analysis, where the correlation coefficient was better than 99.8%. The value of band gap can be obtained by extrapolation of the linear portion of graph to the horizontal axis. The direct band gap was found to be 3.78 eV. This

value is in close agreement with the values reported earlier for NiO thin films [48,49,56]. Therefore, my nickel oxide thin films exhibited the desired optical properties for the dielectric layer in THM applications, i.e. high refractive index and wide band gap.

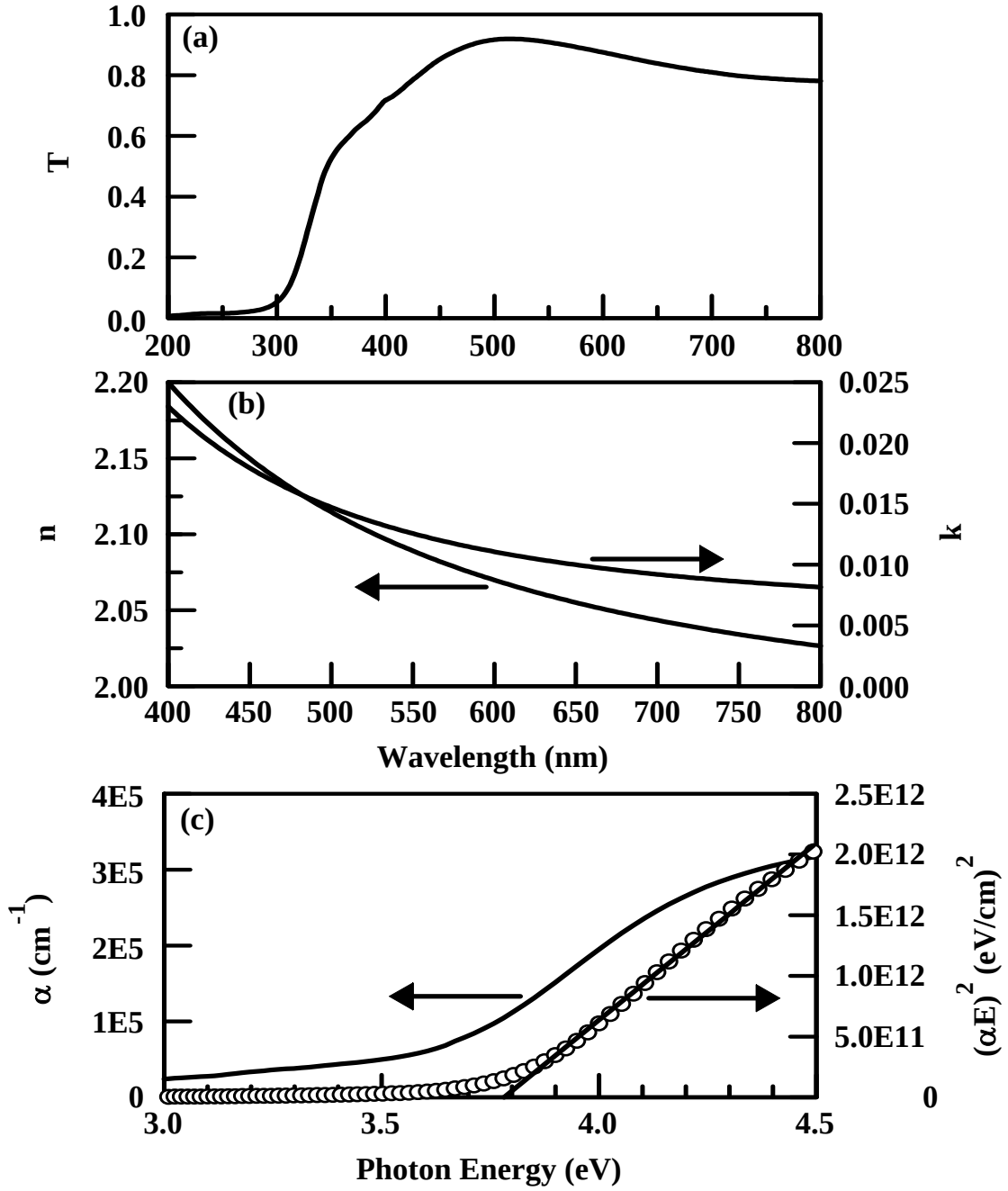

Fig.3.4.(a) Normal-incidence transmittance spectrum of a nickel oxide thin film with a thickness of 120 nm, (b) Dispersion curves of the refractive index (*n*) and extinction coefficient (*k*) of the same film, (c) Absorption coefficient (α) and Tauc plot [$(\alpha E)^2$] of the same film as functions of photon energy (*E*). Parts (a) and (b) have the same horizontal variable (wavelength).

CHAPTER 4: MOLYBDENUM OXIDE THIN FILMS

4.1 Introduction

Molybdenum oxide (MoO_3) is a wide-band-gap metal oxide semiconductor that is characterized by chemical stability, electrochemical activity, and switchable electrical and optical properties [66]. Therefore, it has found potential applications in widely diverse fields, including electrochromic devices and smart windows [67], optical recording [68], resistive switching [69], supercapacitors [70], gas sensing [71], catalysis [72], lithium-based batteries [73], and organic solar cells [74]. A number of techniques have been used to fabricate the molybdenum oxide thin films, such as thermal evaporation [71,75,76], thermal oxidation of molybdenum [75], sputtering [77,78], pulsed laser deposition [72,74], electrodeposition [76], sol-gel deposition [74], chemical vapor deposition [67], and atomic layer deposition [79]. For THM applications, MoO_3 has the desired properties of visible transparency and refractive index. However, its suitability for this application has yet to be investigated.

4.2 Properties of Molybdenum Oxide Thin Films

In this work, molybdenum oxide thin films were prepared by thermal evaporation of MoO_3 powder from a resistively-heated molybdenum boat.

4.2.1 Structural Properties

XRD analysis indicated that the prepared MoO_3 films were amorphous. Figure 4.1(a) shows the XRD pattern of a molybdenum oxide film. The pattern depicts a broad peak, typical of an amorphous structure that was due to the fused silica substrate. No peaks due to MoO_3 were

observed, indicating that the as deposited molybdenum oxide thin films were amorphous. The XRD pattern of the transparent heat mirror (MoO_3/Ag) is shown in Figure 4.1(b), and it exhibits a peak that is due to elemental silver. Figures 4.2 (a) and (b) show representative three-dimensional AFM images of individual molybdenum oxide and silver thin films, respectively. The root mean square surface roughness *(R_{rms})* of the MoO_3 films was 0.54 nm, indicating a smooth surface. The R_{rms} value for the silver films was 3.05 nm, with a peak-to-valley variation of 25 nm, indicating a rough and porous structure.

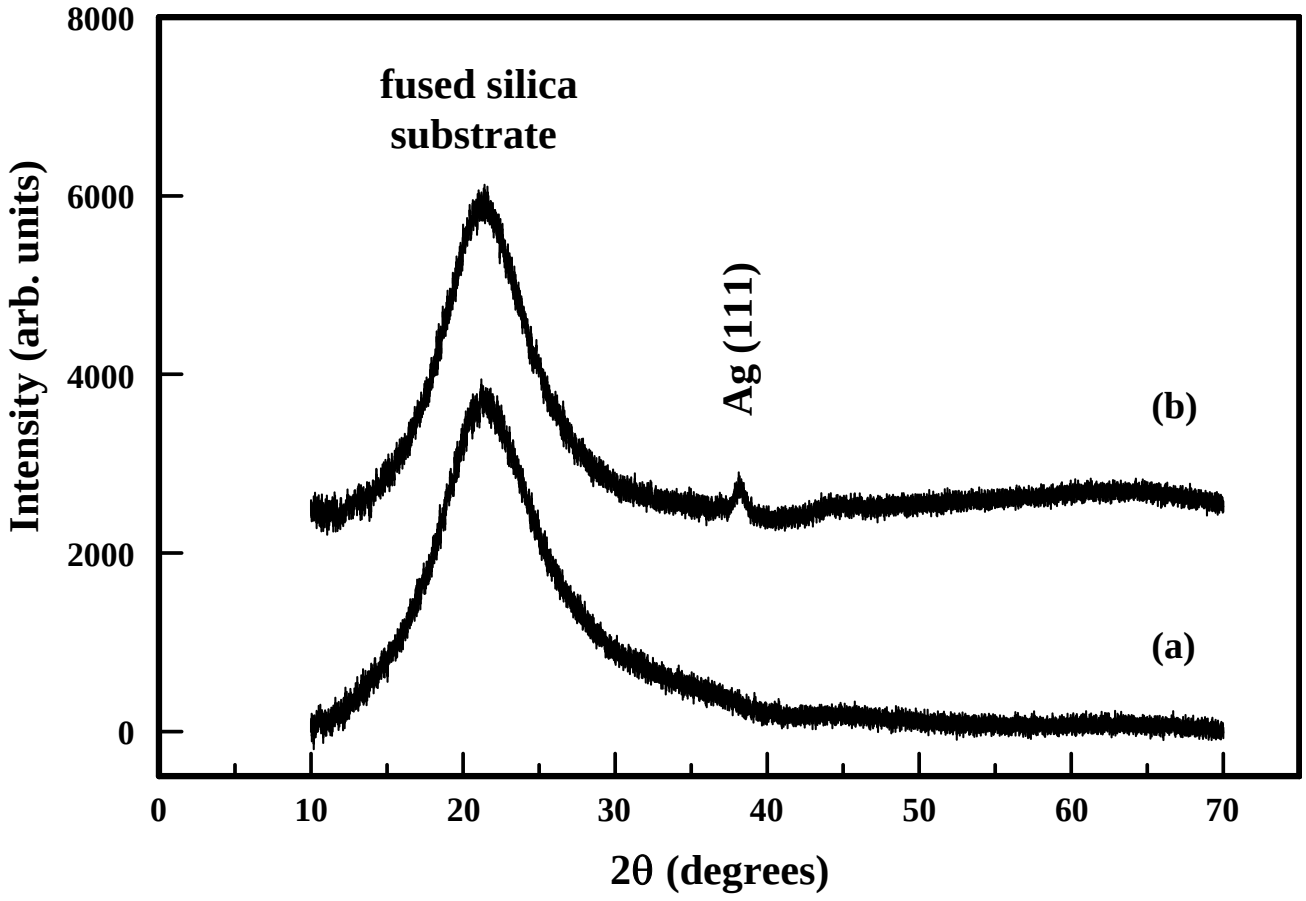

Figure 4.1 XRD spectra: (a) A molybdenum oxide thin film, (b) A transparent heat mirror (consisting of a molybdenum oxide layer on top of a silver layer).

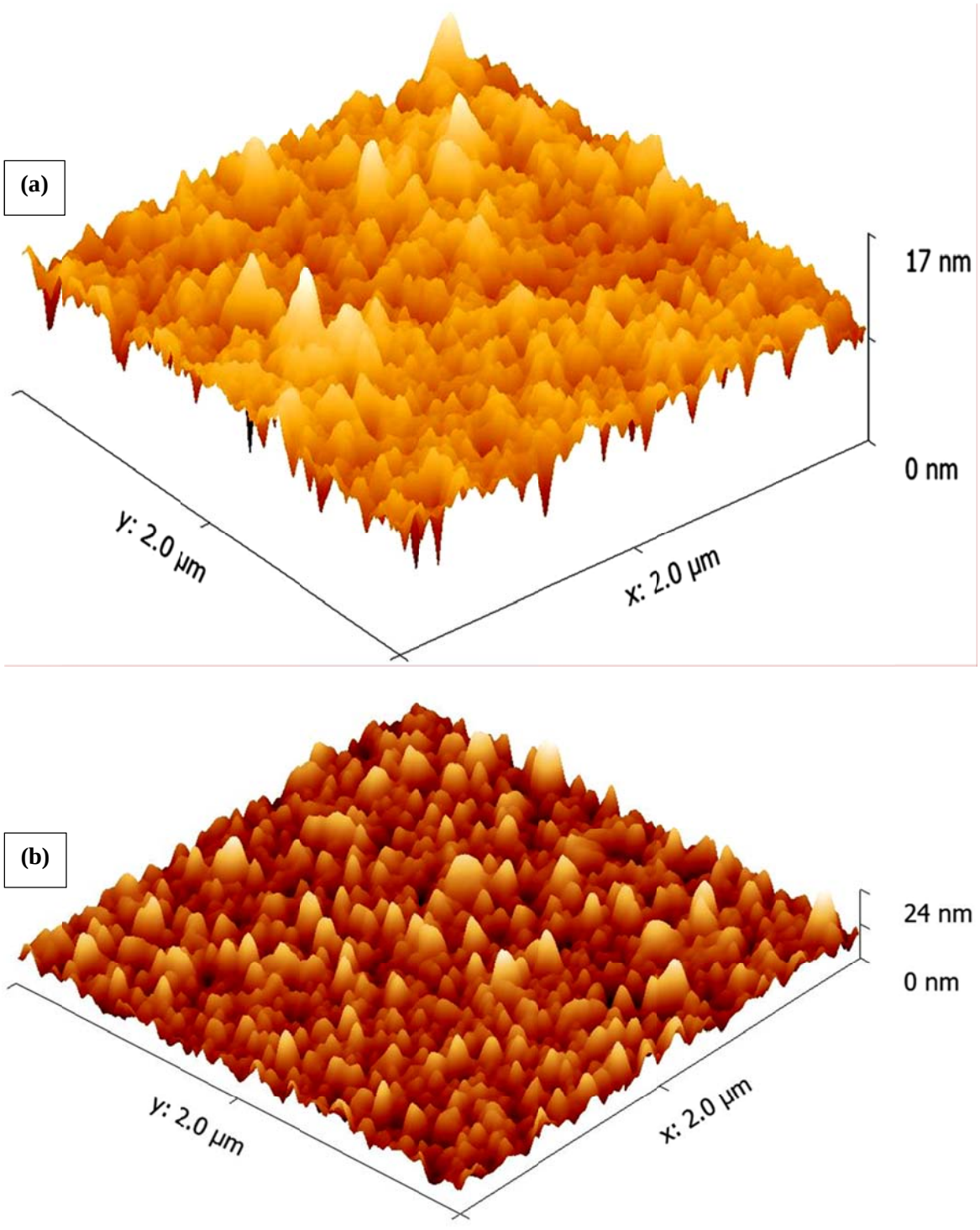

Figure 4.2 Three dimensional AFM micrographs: (a) molybdenum oxide thin film with a thickness of 177 nm, (b) silver thin film with a thickness of 40 nm.

4.2.2 Chemical Properties

The molybdenum XPS 3d core level spectrum consists of two sublevels ($3d_{3/2}$ and $3d_{5/2}$) due to spin-orbit splitting. In MoO_3 (Mo^{6+} oxidation state), the reported values for the binding energy of Mo $3d_{5/2}$ and Mo $3d_{3/2}$ levels are in the ranges 232.2-232.8 eV and 235.4-235.9 eV, respectively [70,71,75,76,78,79]. The O ls spectrum of MoO_3 thin films is mostly asymmetric and has several components, which indicates the existence of several types of oxygen species. Typically, the O ls spectrum in MoO_3 thin films consists of two components. The first component occurs on the low binding energy side in the spectrum and is called the low-binding-energy (LBE) component. This component is attributed to oxygen bound to molybdenum. The second component, high-binding-energy (HBE) component, may be attributed to oxygen species (such as water vapour, OH species, or carbonates) adsorbed at the surface of the film. The reported values of the binding energies of these components are in the range of 530.1-530.5 eV for the LBE component [70,71,75,78,79], and 532 eV for the HBE component [75,78].

XPS spectra of the MoO_3 film were obtained in the Mo 3d and O ls core level regions, and are shown in Figure 4.3. In order to determine the binding energies of the Mo $3d_{5/2}$ and Mo $3d_{3/2}$ levels, the Mo 3d spectrum was deconvoluted using a non-linear least squares algorithm with a Shirley background and a Gaussian—Lorentzian mixed line shape. The binding energies of the Mo $3d_{5/2}$ and the Mo $3d_{3/2}$ peaks were 232.7 eV and 235.8 eV, respectively. These values match those of Mo in the Mo^{6+} oxidation state, indicating that our films were stoichiometric. Another indication of the stoichiometry of the films is the intensity ratio of the Mo $3d_{3/2}$ peak to the Mo $3d_{5/2}$ peak, which was 0.64, in perfect agreement with the value reported in the literature for MoO_3 [71]. The O ls spectrum was resolved into the two components LBE and HBE, as

shown in Figure 4.3(b). The binding energies of these two components were 530.6 eV and 531.4 eV, respectively. The ratio of the HBE component to the total O 1s peak was 0.19. Finally, the energy difference (Δ) between the Mo $3d_{5/2}$ and the O 1s LBE component was 297.9 eV, in perfect agreement with the value reported in the literature for stoichiometric MoO_3[70,78,79].

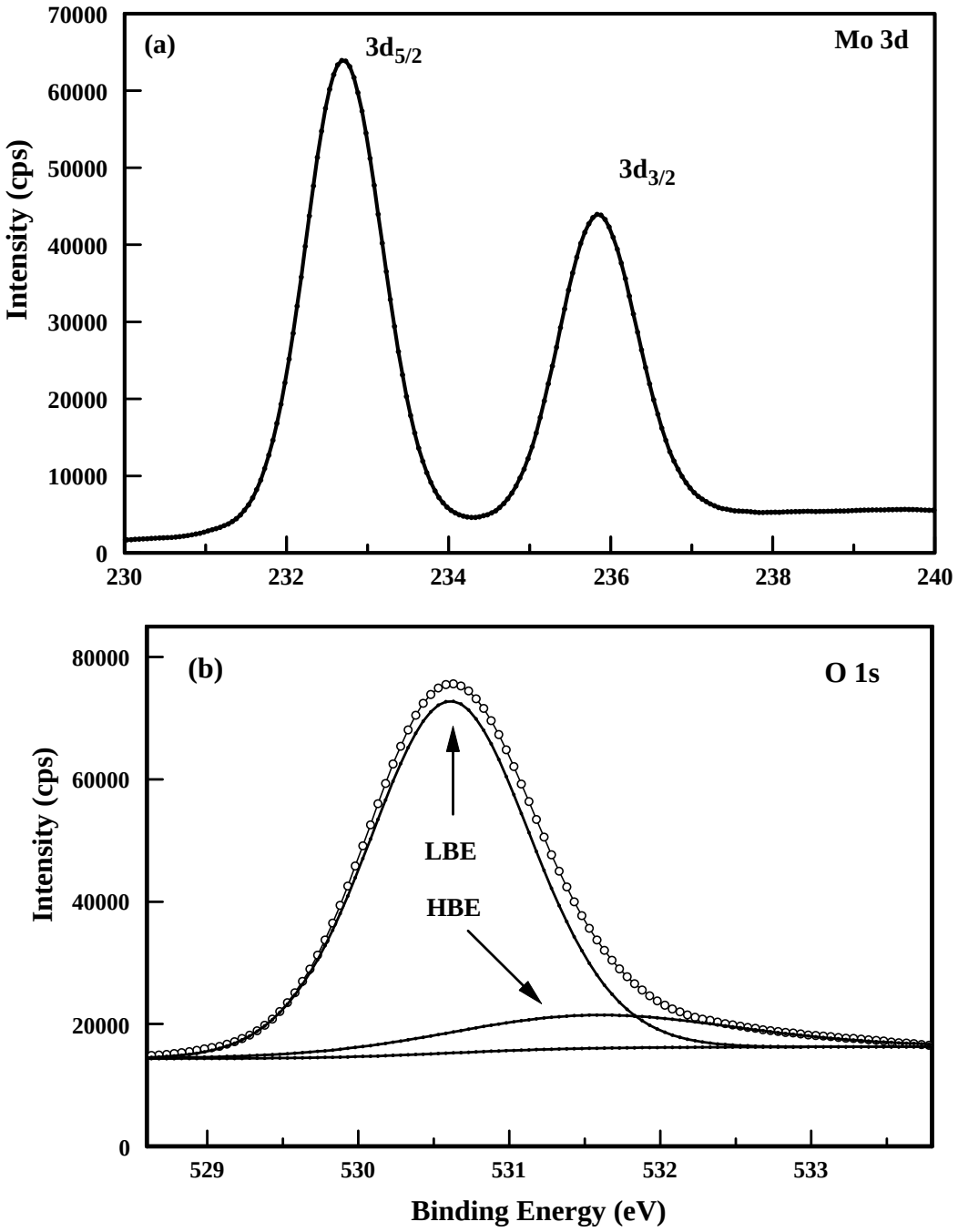

Figure 4.3 XPS spectra of molybdenum oxide thin films: (a) Mo 3d core level spectrum, (b) O 1s core level spectrum. The O1s spectrum was resolved into a low-binding energy component (LBE) and a high-binding-energy component (HBE), where the experimental spectra are represented by the open circles.

4.2.3 Optical Properties

The normal-incidence transmittance spectrum of a MoO_3 film is shown in Figure 4.4(a). This spectrum was used to calculate the optical constants of the film using the procedure discussed in section 3.3, except that the extinction coefficient of the films was taken to be constant (k_o). The best-fit parameters were n_o = 1.99, $A_1 = 2.86 \times 10^3$ nm^2, $A_2 = 6.72 \times 10^9$ nm^4, d = 177 nm, and $k_o = 1.87 \times 10^{-3}$. These parameters were used to calculate the refractive index of the films, whose dispersion curve is shown in Figure 4.4(b). Reported values of the refractive index of molybdenum oxide thin films are in the range 1.8-2.3 [67,76,77]. The values reported in this work are in close agreement with those reported for thermally evaporated MoO_3 [76]. Taking n =2.076 and n_b=2.161 at λ= 550 nm [80], the relative density of the films was estimated to be 0.95. The absorption coefficient and band gap are shown in Figure 4.4(c), where the band gap was found to be 2.82 eV. In the case of MoO_3 films, the best-fit was obtained with $\eta = 2$, indicating an indirect band gap. The reported values of the band gap of MoO_3 thin films are in the range 2.69-3.27 eV [67,71,77]. Therefore, my MoO_3 films exhibited the desired optical properties for the dielectric layer in THM applications.

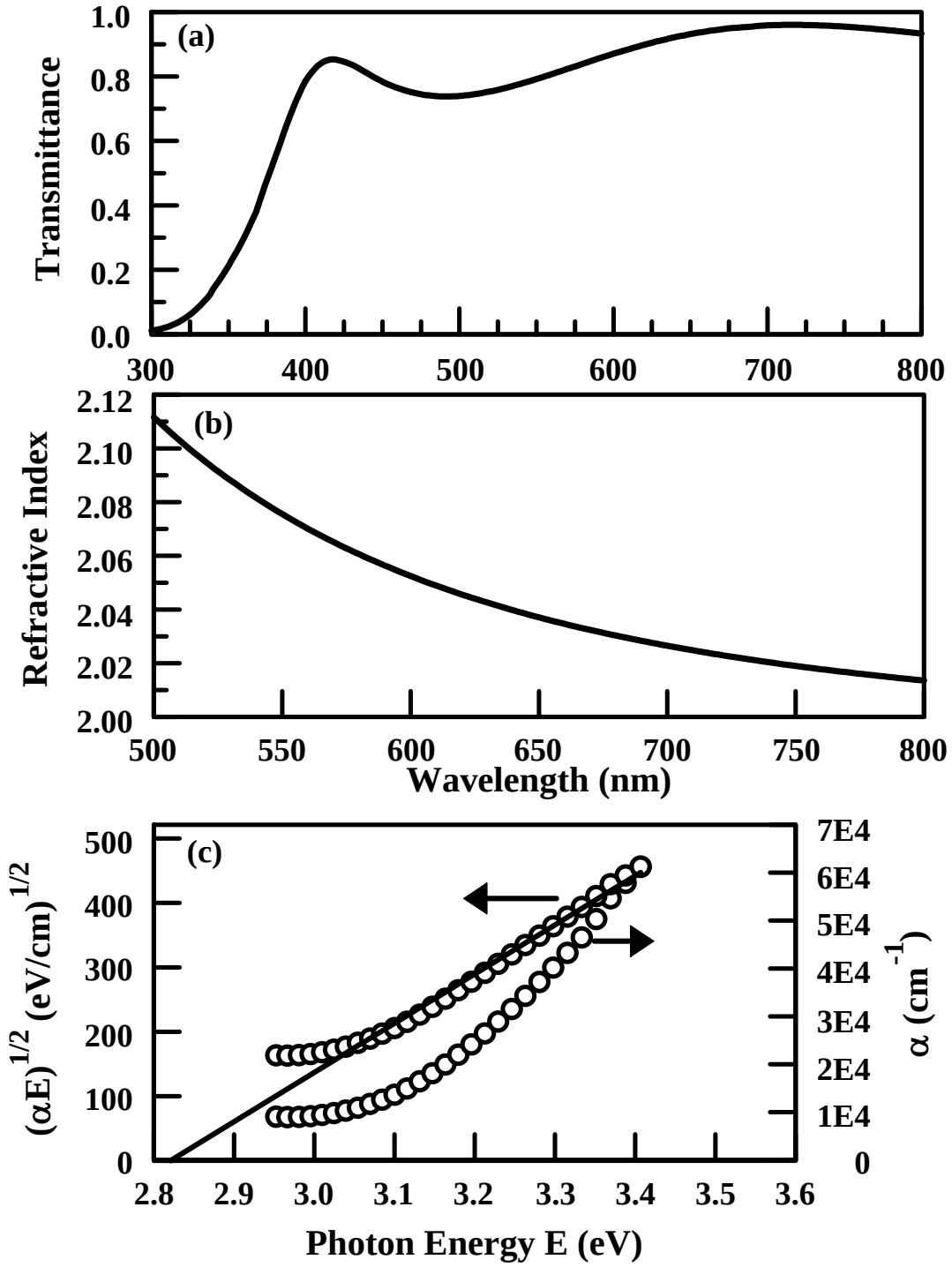

Figure 4.4 (a) Normal-incidence transmittance spectrum of a molybdenum oxide thin film of thickness 177 nm, **(b)** Dispersion curve of the refractive index of the same film, **(c)** Absorption coefficient (α) and Tauc plot of the same film as functions of photon energy.

CHAPTER 5: CHROMIMIUM OXIDE THIN FILMS

5.1 Introduction

Chromium can exist in several oxidation states. Among them, Cr_2O_3 is the most stable thermodynamic phase [81,82]. This material possesses unique characteristics, such as hardness, wear and oxidation resistance, chemical inertness, low friction coefficient, and visible transparency [81-83]. Cr_2O_3 thin films have found diverse applications in several fields, such as protective coatings, catalysis, liquid crystal displays and electrochromic coatings, solar energy collection, and organic solar cells [82-87]. Several techniques have been used to fabricate Cr_2O_3 thin films, including chemical vapor deposition [81,82,84,86], sputtering [83,87], pulsed laser deposition [85], and oxidation of chromium [88].

5.2 Properties of Chromium Oxide Thin Films

In this work, chromium oxide thin films were deposited by the reactive electron-beam evaporation of pure Cr_2O_3 pellets under an oxygen partial pressure of 5×10^{-4} mbar.

5.2.1 Structural Properties

Figure 5.1(a) shows the XRD pattern of a chromium oxide film. The pattern depicts a broad peak, typical of an amorphous structure that was due to the fused silica substrate. No peaks due to Cr_2O_3 were observed, indicating that the as deposited chromium oxide thin films were amorphous. The XRD pattern of the transparent heat mirror (Cr_2O_3/Ag) is shown in Figure 5.1(b), and it exhibits a peak that is due to elemental silver.

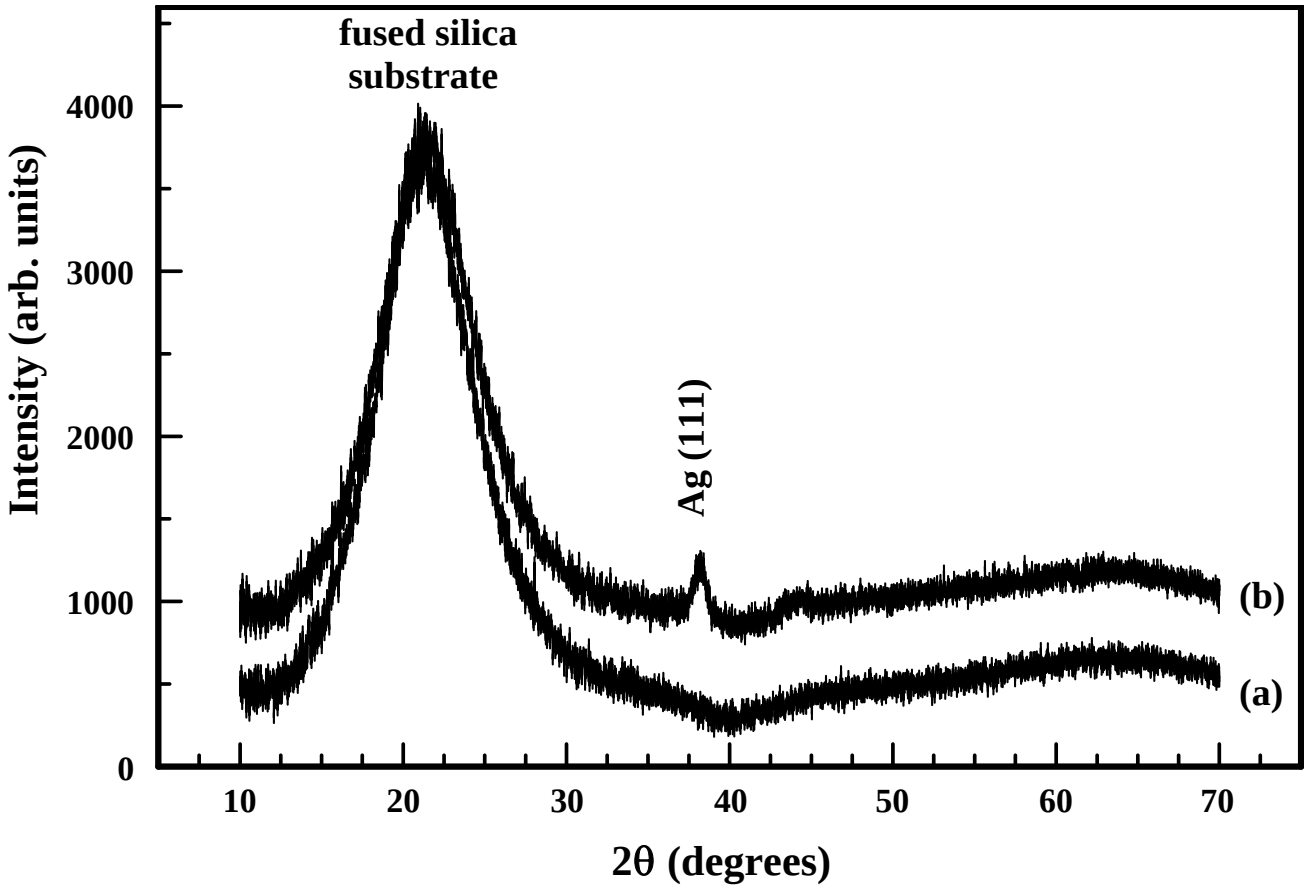

Figure 5.1 XRD spectra: (a) A chromium oxide thin film, (b) A transparent heat mirror (consisting of a chromium oxide layer on top of a silver layer).

Figures 5.2 (a and b) show representative three-dimensional AFM images of individual chromium oxide and silver thin films, respectively. The surfaces exhibited a columnar structure. The root-mean-square surface roughness (R_{rms}) of the chromium oxide films was 1.25 nm, indicating a smooth surface. The R_{rms} value for the silver films was 2.80 nm, indicating a rough and porous structure.

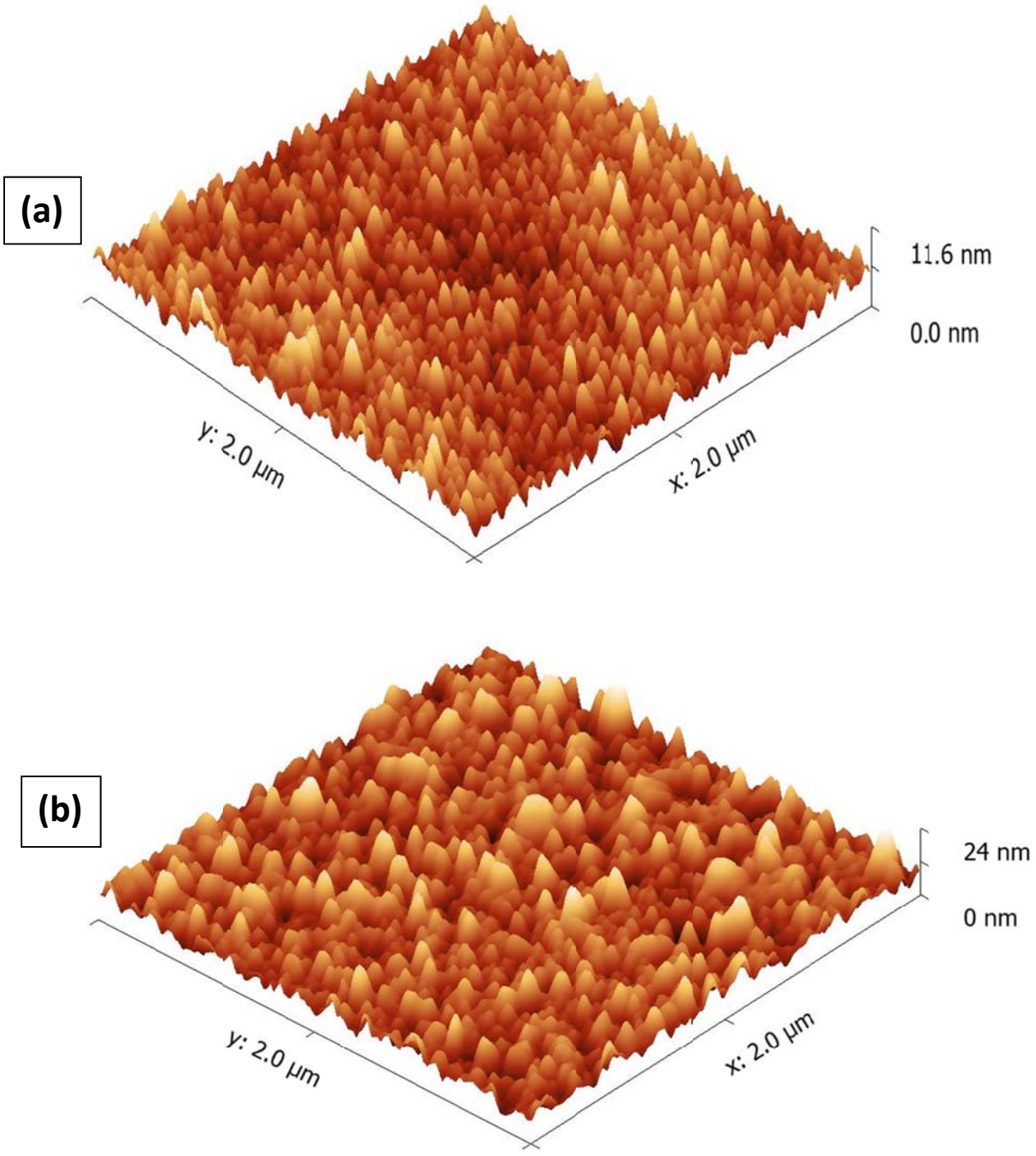

Figure 5.2 Three dimensional AFM micrographs: (a) chromium oxide thin film with a thickness of 158 nm, (b) silver thin film with a thickness of 20 nm.

5.2.2 Chemical Properties

The chemical state and chemical composition of the films were investigated using XPS. The chromium XPS 2p core level spectrum consists of two sublevels ($2p_{1/2}$ and $2p_{3/2}$) due to spin-orbit splitting. The Cr $2p_{3/2}$ spectrum is very complex and asymmetric, possibly due to the existence of several oxidation states, multiplet splitting, and 3d shake-up satellites [88]. Similarly, the O 1s core level spectrum is asymmetric due to the existence of several oxidation states and/or adsorbed oxygen species (such as water, hydroxyl group, or carbonates) that may be present at the surface of the film due to its exposure to the atmosphere. Figure 5.3 shows XPS core level spectra of my chromium oxide thin films in the Cr $2p_{3/2}$ and O 1s regions. The spectra were deconvoluted into several components using a non-linear least squares algorithm with a Shirley background and a Gaussian—Lorentzian mixed line shape. The binding energies and weights of these components are given in Table 5.1. The Cr $2p_{3/2}$ spectrum was resolved into four components. These components may arise from multiplet splitting in Cr_2O_3 [89]. All the components were assigned to Cr_2O_3, as was also reported by Kirby *et al.* [88]. The O 1s spectrum was resolved into two components: the low-binding-energy (LBE) component assigned to oxygen bonded to chromium in Cr_2O_3 [88], and the high-binding-energy (HBE) component was assigned to adsorbed oxygen species. An indicator of the stoichiometry of the films is the binding energy difference (Δ) between the Cr $2p_{3/2}$ and O 1s peaks, which is a suitable parameter to evaluate the valence state of chromium oxide, as was done for other oxides [79]. In my films, this value was $\Delta = 46.5$ eV, which is close to the reported value of 46.2 eV for Cr_2O_3 [88].

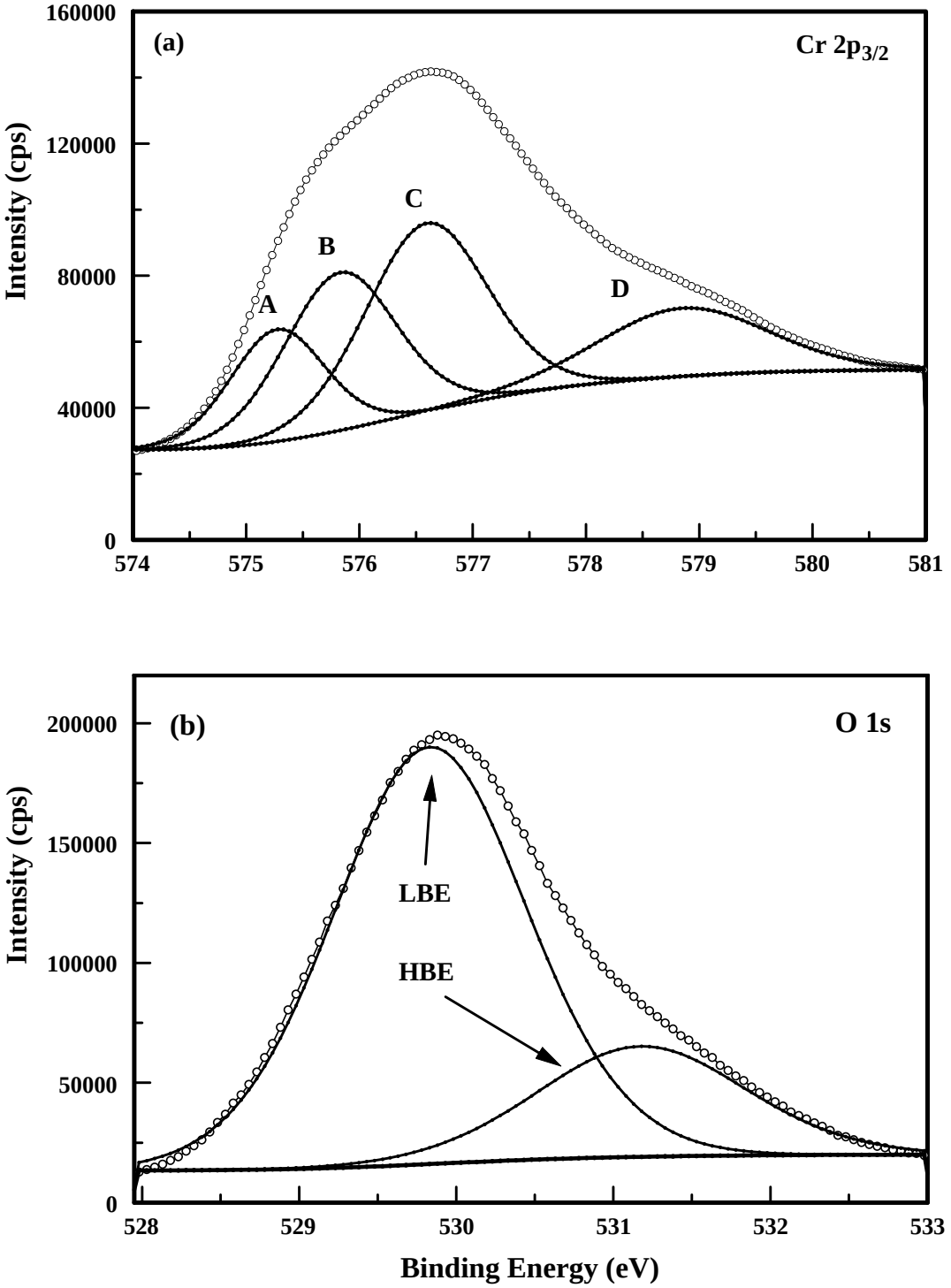

Figure 5.3 XPS spectra of chromium oxide thin films: (a) Cr $2p_{3/2}$ core level spectrum, (b) O 1s core level spectrum. The experimental spectra are represented by the open circles. The spectra were deconvoluted into their component peaks.

Table 5.1 Summary of the XPS analysis of individual chromium oxide thin films

Peak	Component	BE (eV)	Γ (eV)	%W	Assignment
Cr $2p_{3/2}$	A	575.3	1.0	17	Cr_2O_3
	B	575.8	1.2	28	Cr_2O_3
	C	576.6	1.3	37	Cr_2O_3
	D	578.9	1.8	18	Cr_2O_3
O 1s	LBE	529.8	1.5	78	Cr_2O_3
	HBE	531.2	1.6	22	

B.E=Binding Energy, Γ=Full width at half maximum, W=Weight of the component

5.2.3 Optical Properties

The normal-incidence transmittance spectrum of a chromium oxide thin film is shown in Figure 5.4(a). This spectrum was used to calculate the optical constants of the film using the procedure presented in section 3.3. The best-fit parameters were $n_o = 1.77$, $A_1 = 3.94 \times 10^3$ nm^2, $A_2 = 4.74 \times 10^9$ nm^4, $k_o = 1.45 \times 10^{-2}$, $B = 4.50 \times 10^6$ nm^3, and $d = 158$ nm. These parameters were used to calculate the refractive index and extinction coefficients of the films, whose dispersion curves are shown in Figure 5.4(b). Taking $n = 1.838$ and $n_b = 2.551$ at $\lambda = 550$ nm [65], the relative density of the films was estimated to be 0.68. The absorption coefficient is shown in Figure 5.4(c). For band gap calculations, both direct and indirect band gaps were tried. For example, Figure 5.4(c) shows a plot of $(\alpha E)^2$ as a function of photon energy. The band gaps of the films were found to be 3.8 eV and 2.5 eV, for the direct and indirect band gap, respectively. The reported values of the direct band gap of Cr_2O_3 lie in the range 3.66-3.83 eV [83,87], and those of the indirect band gap lie in the range 2.4-3.55 eV [90].

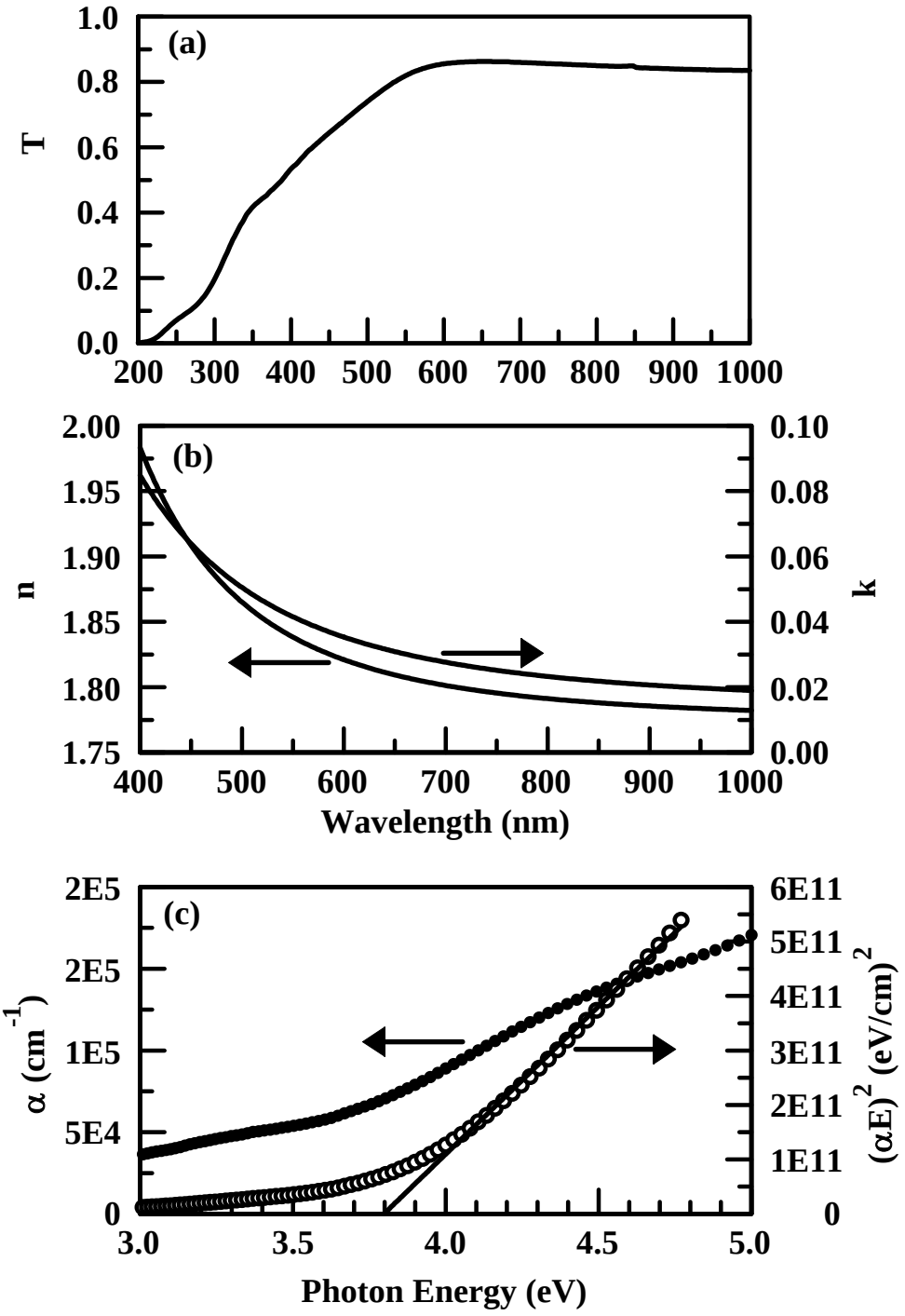

Figure 5.4 (a) Normal-incidence transmittance spectrum of a chromium oxide thin film with a thickness 158 nm, (b) Dispersion curves of the refractive index (*n*) and extinction coefficient (*k*) of the same film, (c) Absorption coefficient (α) and Tauc plot [$(\alpha E)^2$] of the same film as functions of photon energy (E). Parts (a) and (b) have the same horizontal variable (wavelength).

CHAPTER 6: VANADIUM OXIDE THIN FILMS

6.1 Introduction

Multivalency [91-94], wide band gap [95-97], layered structure [98], good chemical and thermal stability [97,99,100], and excellent thermoelectric properties [96,101-103] are the characteristics that make vanadium pentoxide (V_2O_5) a promising material for microelectronic, optoelectronic and electrochemical devices. V_2O_5 thin films have found diverse applications in technological fields, such as thermal and phase dependent electrical switches, optical switches, lithium batteries, electronic information displays, artificial muscles, smart windows, memory devices, and infrared detectors [91-98]. Vanadium oxide thin films have been deposited by a variety of techniques, such as thermal oxidation of vanadium [91,95], thermal evaporation [92,100,101], spray pyrolysis [93], sputtering [94,102], electron beam evaporation [95-97,99], chemical vapor deposition [98], sol-gel deposition [103,104], and pulsed laser deposition [105]. For THM applications, V_2O_5 has the desired properties of visible transparency and refractive index. However, its suitability for this application has yet to be investigated.

6.2 Properties of Vanadium Oxide Thin Films

In this work, vanadium oxide thin films were fabricated by thermal evaporation of V_2O_5 powder from a resistively-heated tungsten boat.

6.2.1 Structural Properties

Figure 6.1(a) shows the XRD pattern of a vanadium oxide film. The pattern depicts a broad peak, characteristic of an amorphous structure, that was due to the fused silica substrate. No peaks due to V_2O_5 were observed, indicating that the as deposited vanadium oxide thin films were amorphous. The XRD pattern of the transparent heat mirror (V_2O_5/Ag) is shown in Figure 6.1(b), and it exhibits a peak that is due to elemental silver.

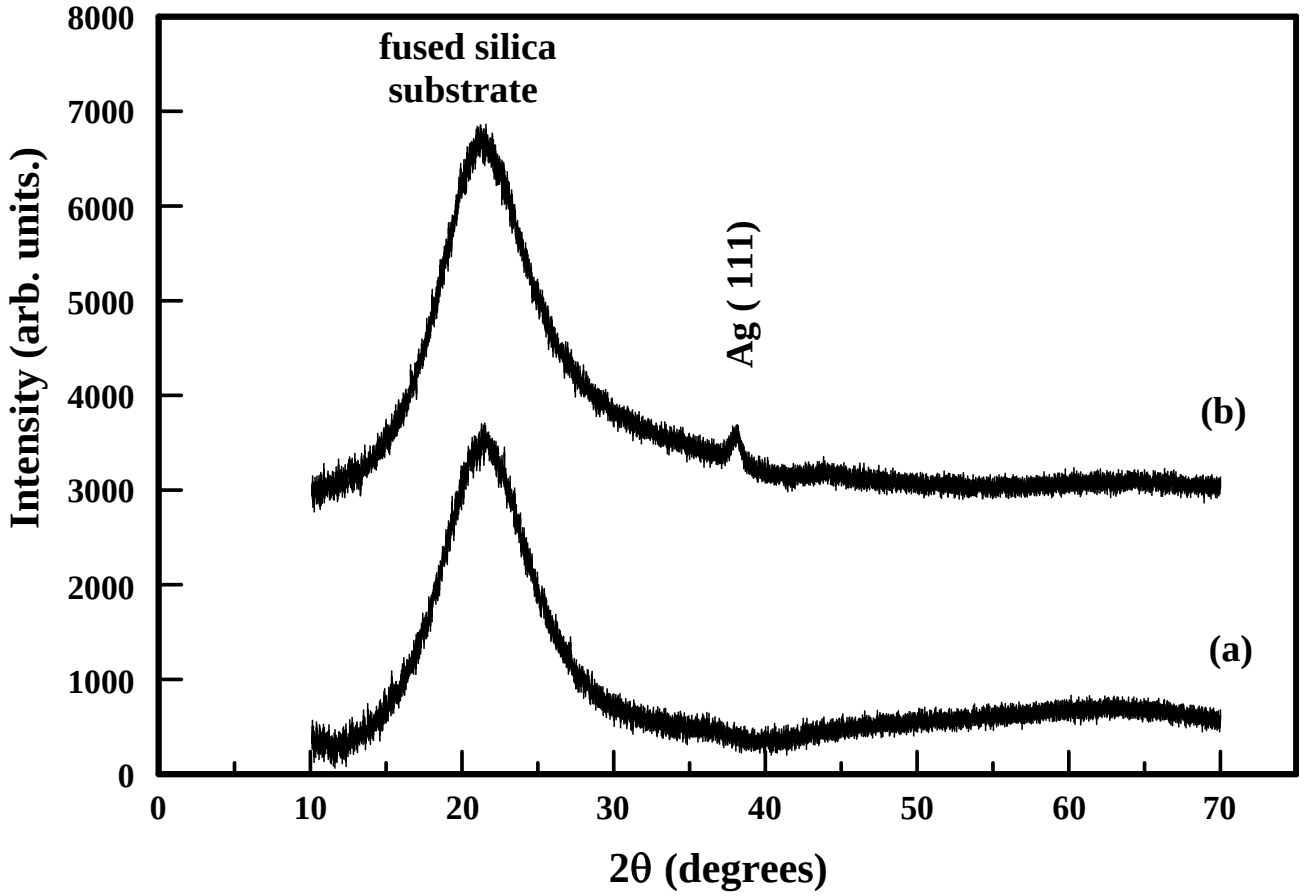

Figure 6.1 XRD spectra: (a) A vanadium oxide thin film, (b) A transparent heat mirror (consisting of a vanadium oxide layer on top of a silver layer).

Figures 6.2 (a and b) show representative three-dimensional AFM images of individual vanadium oxide and silver thin films, respectively. The surfaces exhibited a columnar structure. The root mean square surface roughness (R_{rms}) of the vanadium oxide films was 1.24 nm, and that of silver was 3.05 nm, with a peak-to-valley variation of 25 nm, indicating a rough and porous structure.

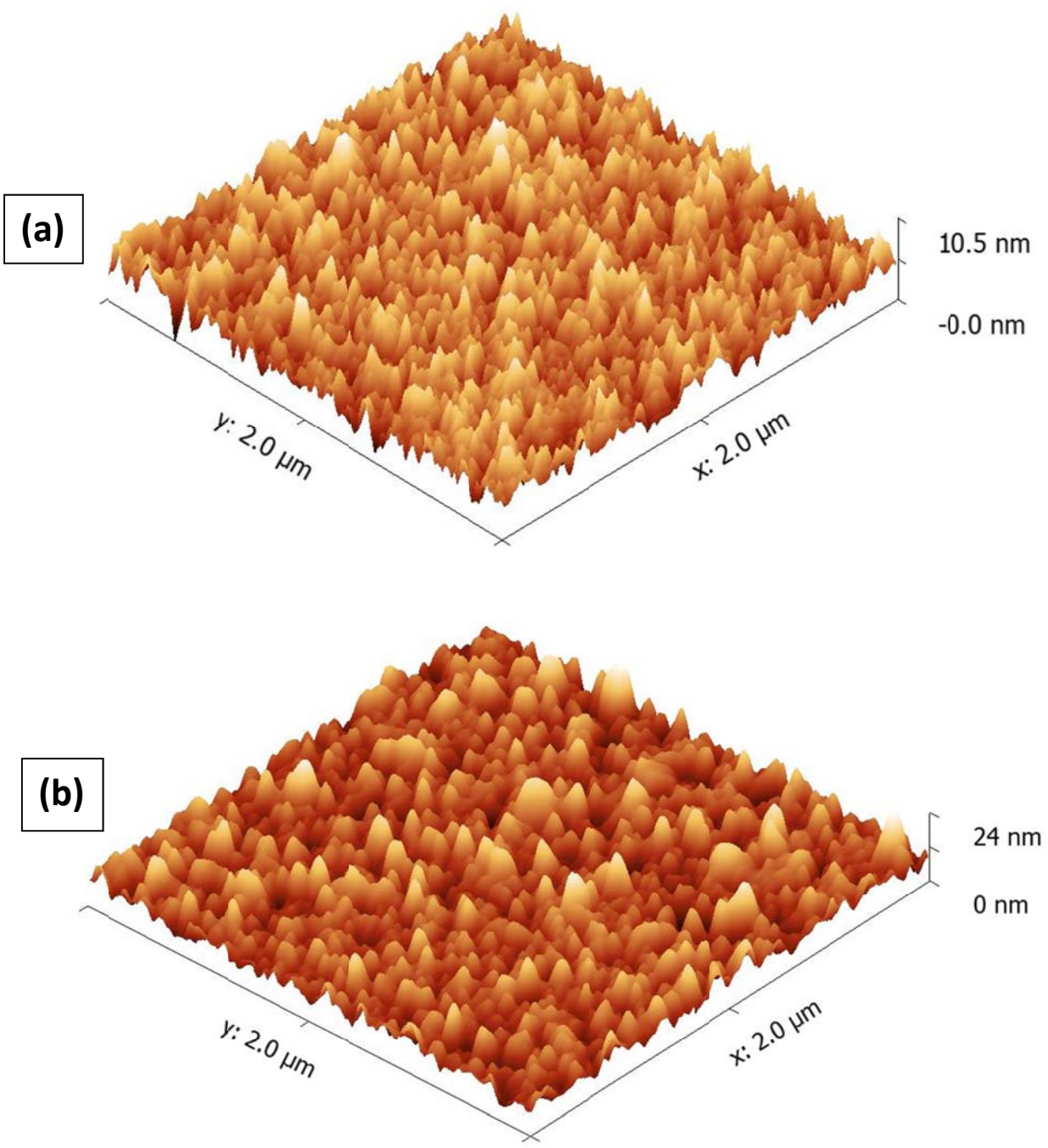

Figure 6.2 Three dimensional AFM micrographs: (a) Vanadium oxide thin film with a thickness of 158 nm, (b) silver thin film with a thickness of 40 nm.

6.2.2 Chemical Properties

The chemical state and chemical composition of the films was investigated using XPS. The vanadium XPS 2p core level spectrum consists of two sublevels ($2p_{1/2}$ and $2p_{3/2}$) due to spin-orbit splitting. Similarly, the O1s core level spectrum is asymmetric due to the existence of several oxidation states and/or adsorbed oxygen species (such as water, hydroxyl group, or carbonates) that may be present at the surface of the film due to its exposure to the atmosphere. Figure 6.3 shows XPS core level spectra of the vanadium oxide thin films in the V $2p_{3/2}$ and O1s regions. The spectra were deconvoluted into several components using a non-linear least squares algorithm with a Shirley background and a Gaussian—Lorentzian mixed line shape. The binding energies and weights of these components are given in Table 6.1. The V $2p_{3/2}$ spectrum was resolved into three components. These components were assigned on the basis of the binding energy values reported in the literature [105-107]. The lowest binding energy peak was assigned to VO_2, whereas the other two components were assigned to V_2O_5, as was also reported by [97-99]. The O1s spectrum was resolved into two components: the low-binding-energy (LBE) component assigned to oxygen bonded to vanadium, and the high-binding-energy (HBE) component assigned to adsorbed oxygen species.

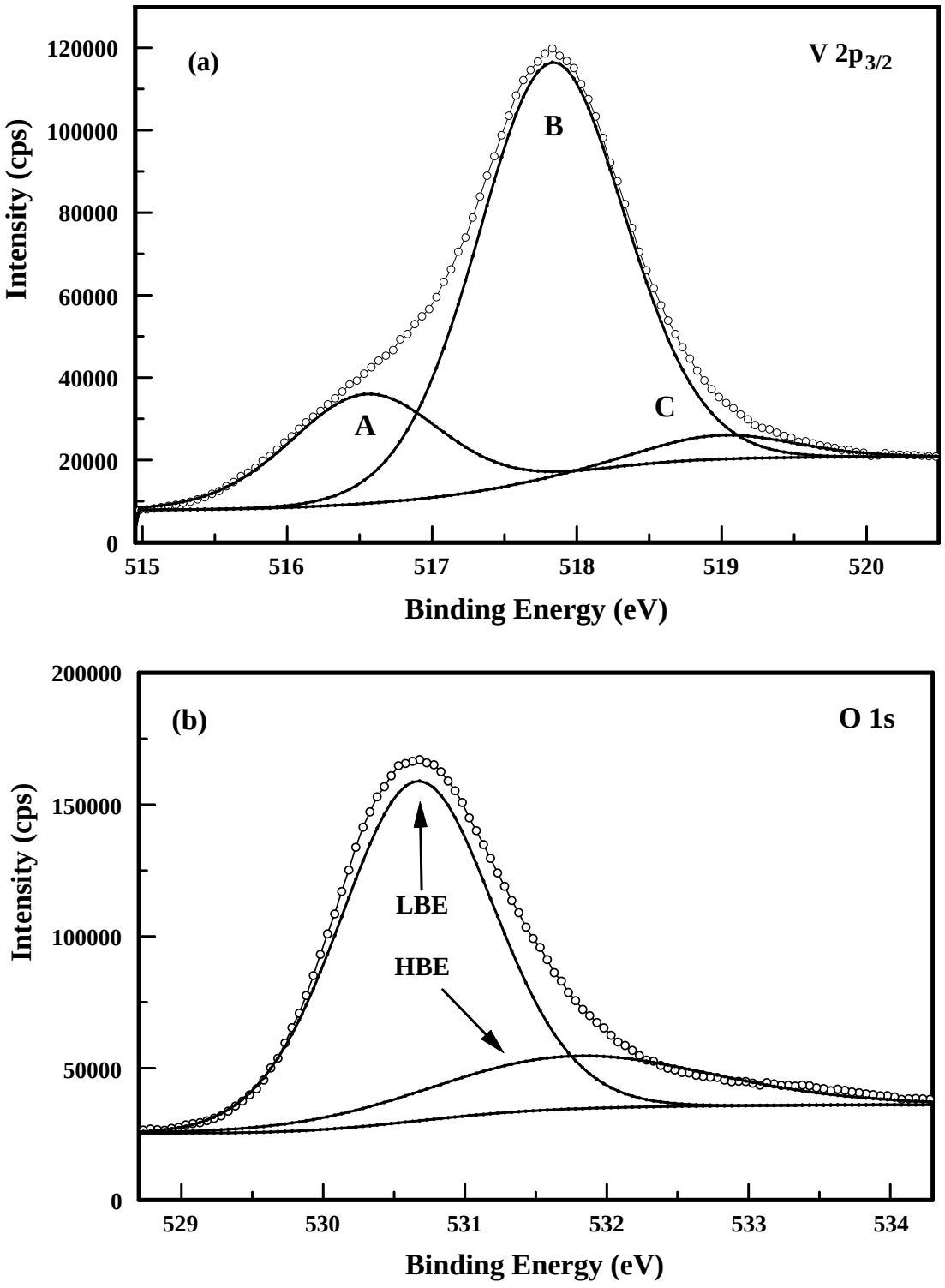

Figure 6.3 XPS spectra of vanadium oxide thin films: (a) V 2p core level spectrum, (b) O1s core level spectrum. The experimental spectra are represented by the open circles.

Table 6.1 Summary of the XPS analysis of individual vanadium oxide thin films

Peak	Component	BE (eV)	Γ (eV)	%W	Assignment
V $2p_{3/2}$	A	516.54	1.23	14.3	VO_2
	B	517.82	1.20	64.2	V_2O_5
	C	518.99	1.19	21.5	V_2O_5
O 1s	LBE	530.66	1.3	78.0	Vanadium Oxide
	HBE	531.75	1.3	22.0	

B.E=Binding Energy, Γ=Full width at half maximum, W=Weight of the component

6.2.3 Optical Properties

The normal-incidence transmittance spectrum of a V_2O_5 thin film is shown in Figure 6.4(a). This spectrum was used to calculate the optical constants of the film using the procedure discussed in section 3.3, except that the extinction coefficient of the films was taken to be constant (k_o). There was an excellent fit of the experimental spectrum by the theoretical model, with a correlation of at least 98.5 %. The best-fit parameters were n_o = 1.54, A_1 = 1.14 × 10^5 nm^2, A_2 = 9.32 × 10^9 nm^4, d = 140 nm, and k_o = 0.0215. These parameters were used to calculate the refractive index of the films, whose dispersion curve is shown in Figure 6.4(b). Reported values of the refractive index of vanadium oxide thin films are in the range 1.9-2.09 [92,96]. The values reported in this work are in close agreement with those reported for thermally evaporated V_2O_5 [92]. Taking n = 2.02 and n_b = 2.40 at λ = 550 nm [108], the relative density of the films was estimated to be 0.83.

To obtain the band gap, $(\alpha E)^{1/\eta}$ was plotted as a function of photon energy, and such a plot is called a Tauc plot. In my film, the best fit was obtained with $\eta = 2$, indicating an indirect band gap. Figure 6.4(c) shows a plot of $(\alpha E)^{1/2}$ as a function of photon energy. The linear portion of the curve was fitted using linear regression analysis, where the correlation coefficient was better than 99.8%. An extrapolation of the linear region of the plot gives the value of the band gap as the intercept to the horizontal axis. The band gap of the film was found to be 2.18 eV. The reported values of the band gap of V_2O_5 thin films are in the range 2.04-3.25 eV [91,95-97].

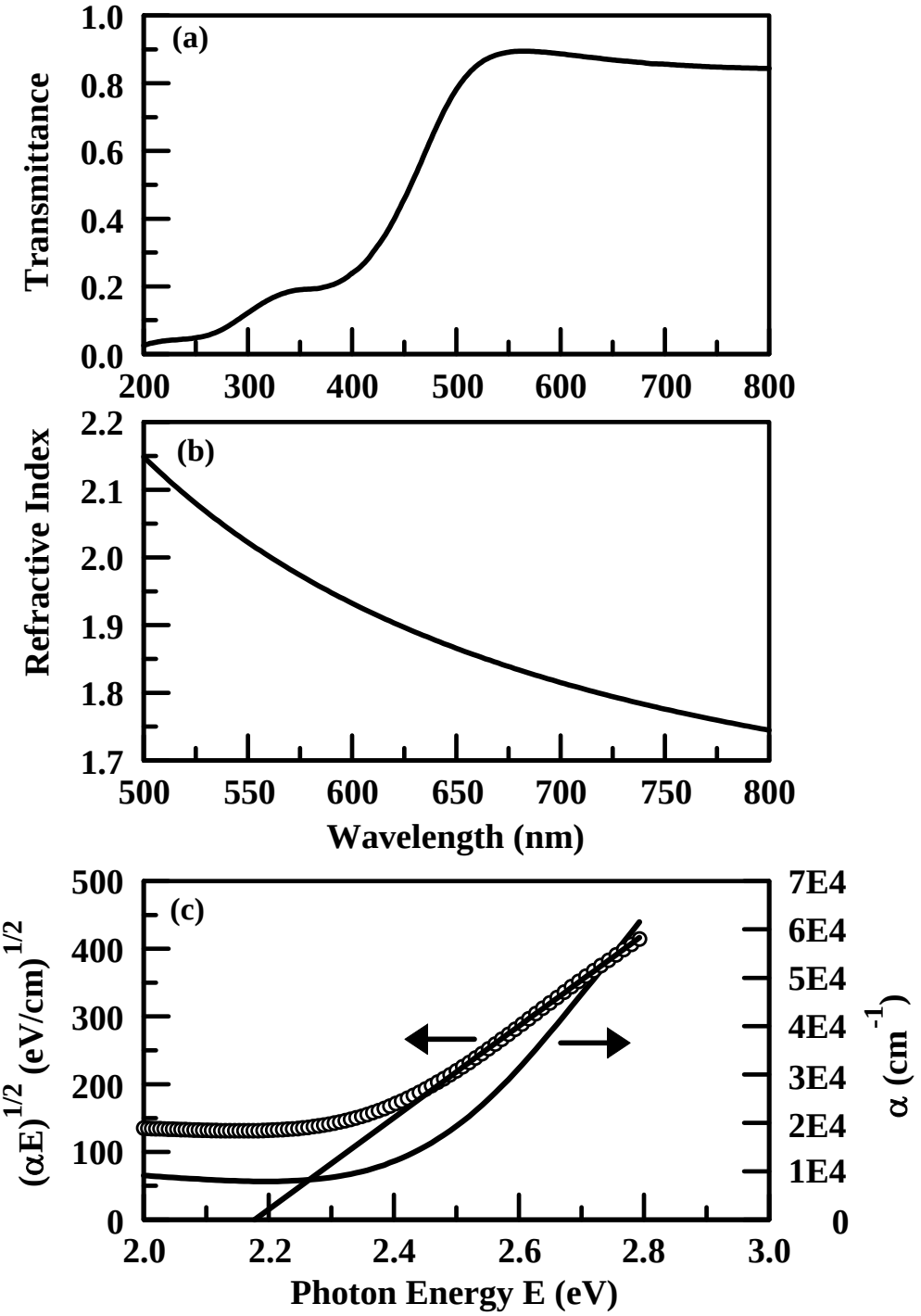

Figure 6.4 (a) Normal-incidence transmittance spectrum of a vanadium oxide thin film of thickness 140 nm, (b) Dispersion curve of the refractive index of the same film, (c) Absorption coefficient (α) and Tauc plot of the same film as functions of photon energy.

CHAPTER 7: TRANSPARENT HEAT MIRRORS

7.1 Optical Properties

The optical spectra of the transparent heat mirrors based on the transition metal oxides considered in this work are shown in Figures 7.1 to 7.4. These THMs exhibited the desired properties of high visible transparency and high infrared reflectance. The maximum transmittance *(T_{max})*, as well as integrated visible transmittance (τ_{vis}) and integrated infrared reflectance *(R_{IR})* are shown in Table 7.1. These quantities are defined as follows:

$$\tau_{vis} = \int_{400}^{700} T(\lambda) d\lambda \qquad (7.1)$$

$$R_{IR} = \int_{700}^{2000} R(\lambda) d\lambda \qquad (7.2)$$

For THM applications, it is desirable to maximize visible transmittance and infrared reflectance. Thus, a simple figure-of-merit (Φ) may be defined as the product of these three parameters as follows:

$$\Phi = T_{\max} \tau_{vis} R_{IR} \qquad (7.3)$$

Values of Φ are listed in Table 7.1. It is evident that the films deposited by thermal evaporation (MoO_3 and V_2O_5) showed better performance than those deposited by e-beam evaporation. This may be attributed to the fact that there was more inter-diffusion among the layers deposited by e-beam evaporation (see section 7.2). On the other hand, the maximum transmittance of the e-beam evaporated films was shifted to the visible range, as desired in THM applications. Evaluation of the THMs on the basis of their solar performance will be presented in section 7.3.

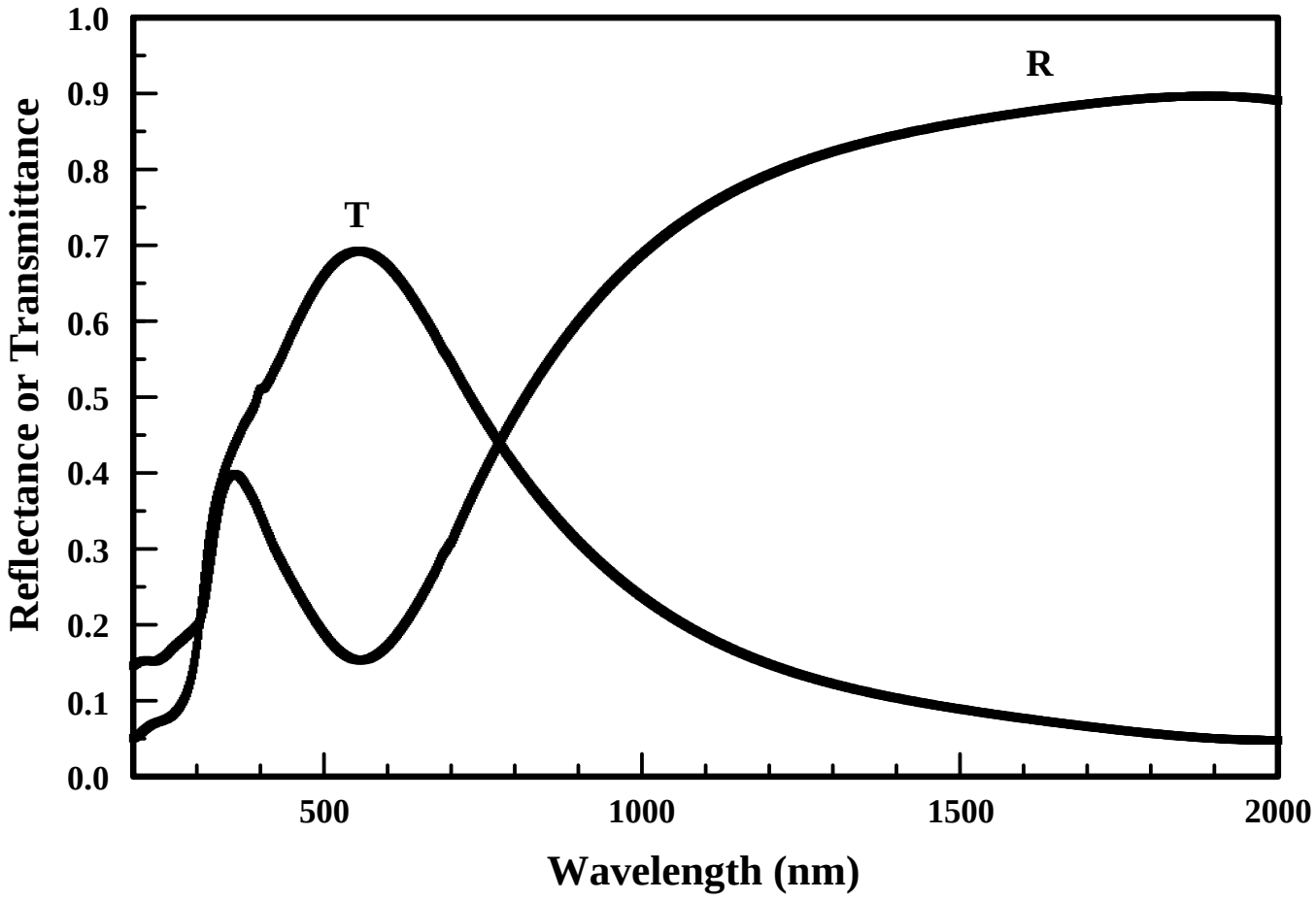

Figure 7.1 Normal-incidence transmittance and reflectance spectra of a transparent heat mirror based on the NiO/Ag structure. The thickness of NiO was 30 nm, and that of silver was 20 nm.

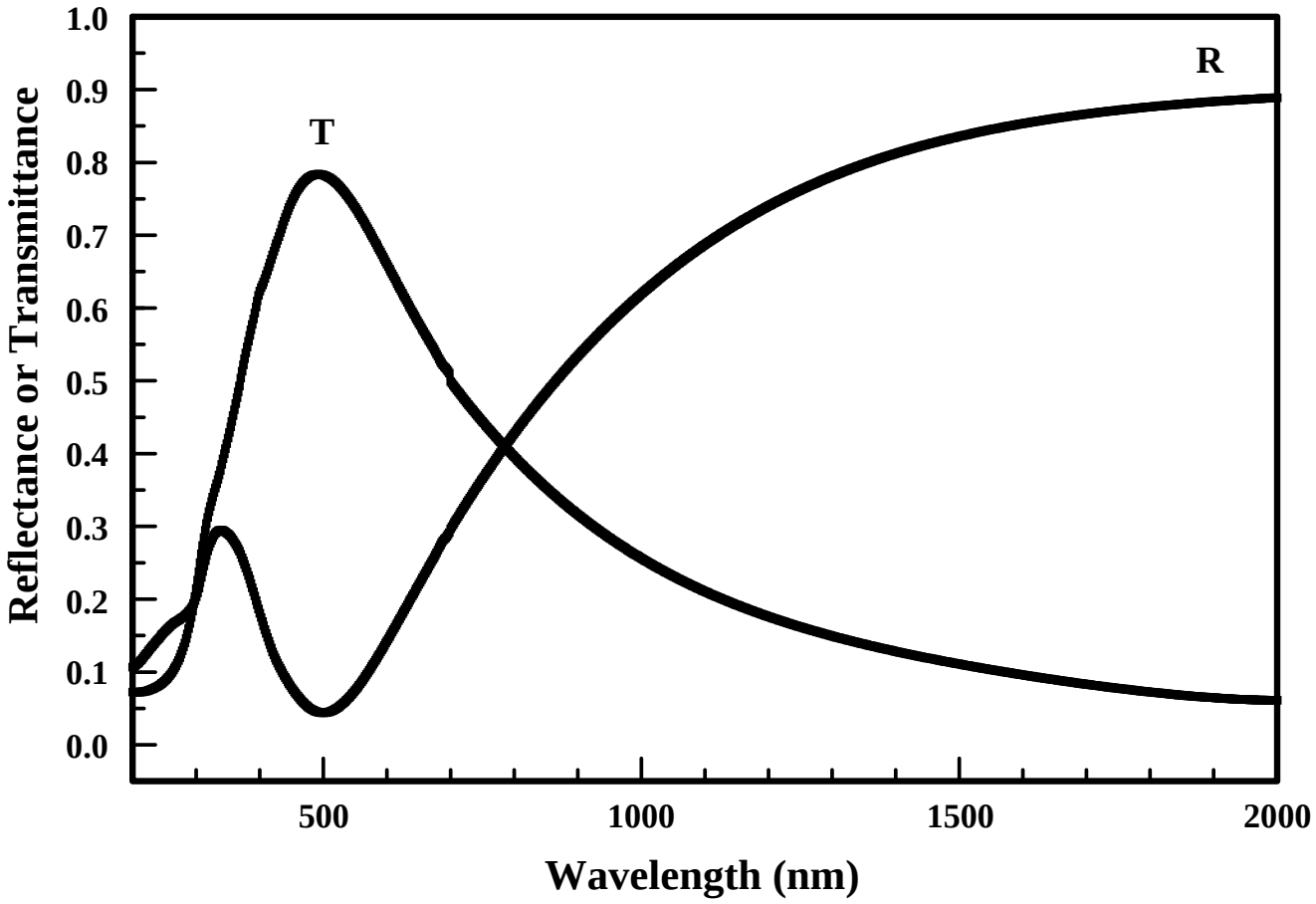

Figure 7.2 Normal-incidence transmittance and reflectance spectra of a transparent heat mirror based on the MoO_3/Ag structure. The thickness of MoO_3 was 40 nm, and that of silver was 40 nm.

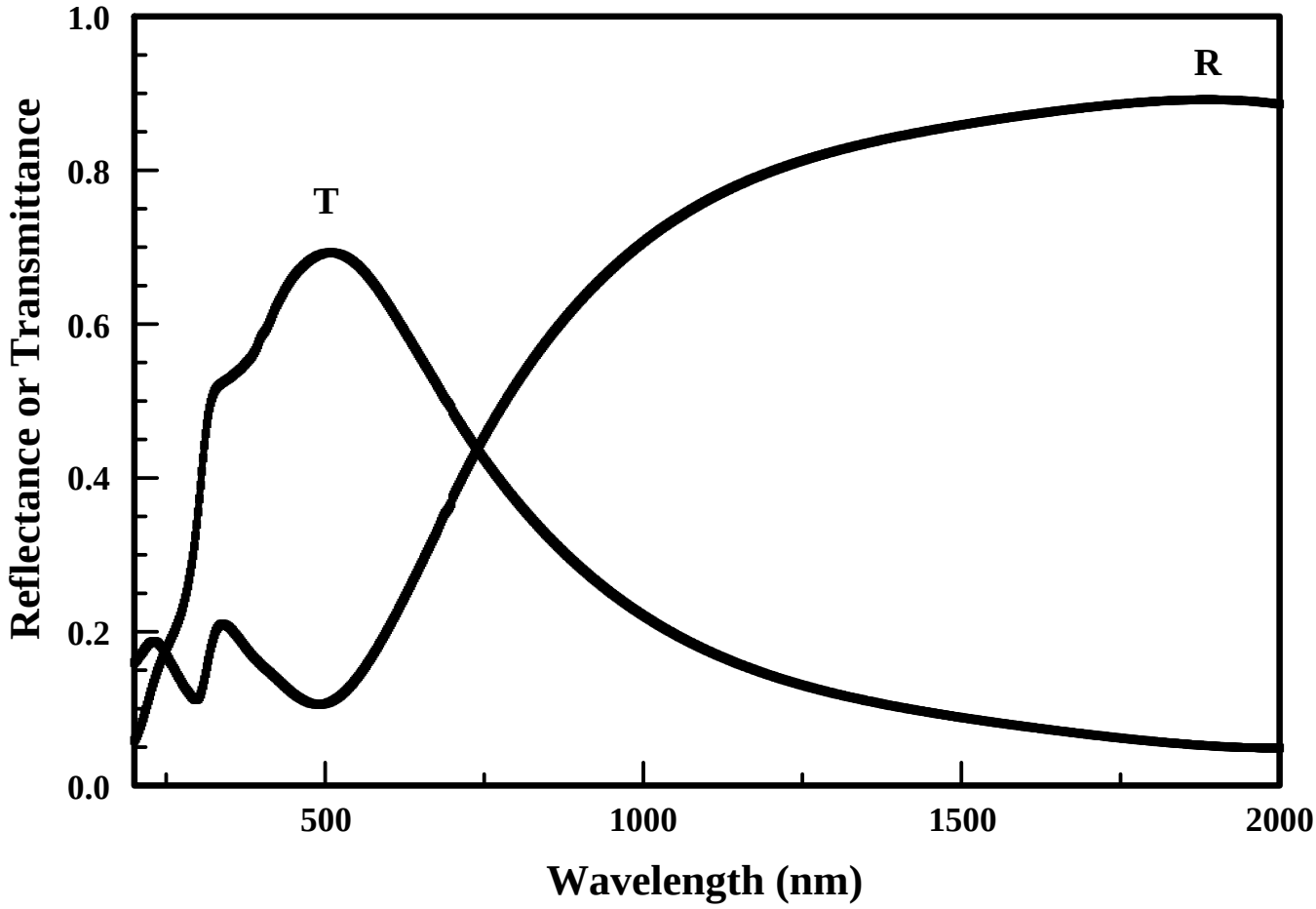

Figure 7.3 Normal-incidence transmittance and reflectance spectra of a transparent heat mirror based on the Cr_2O_3/Ag structure. The thickness of Cr_2O_3 was 40 nm, and that of silver was 20 nm.

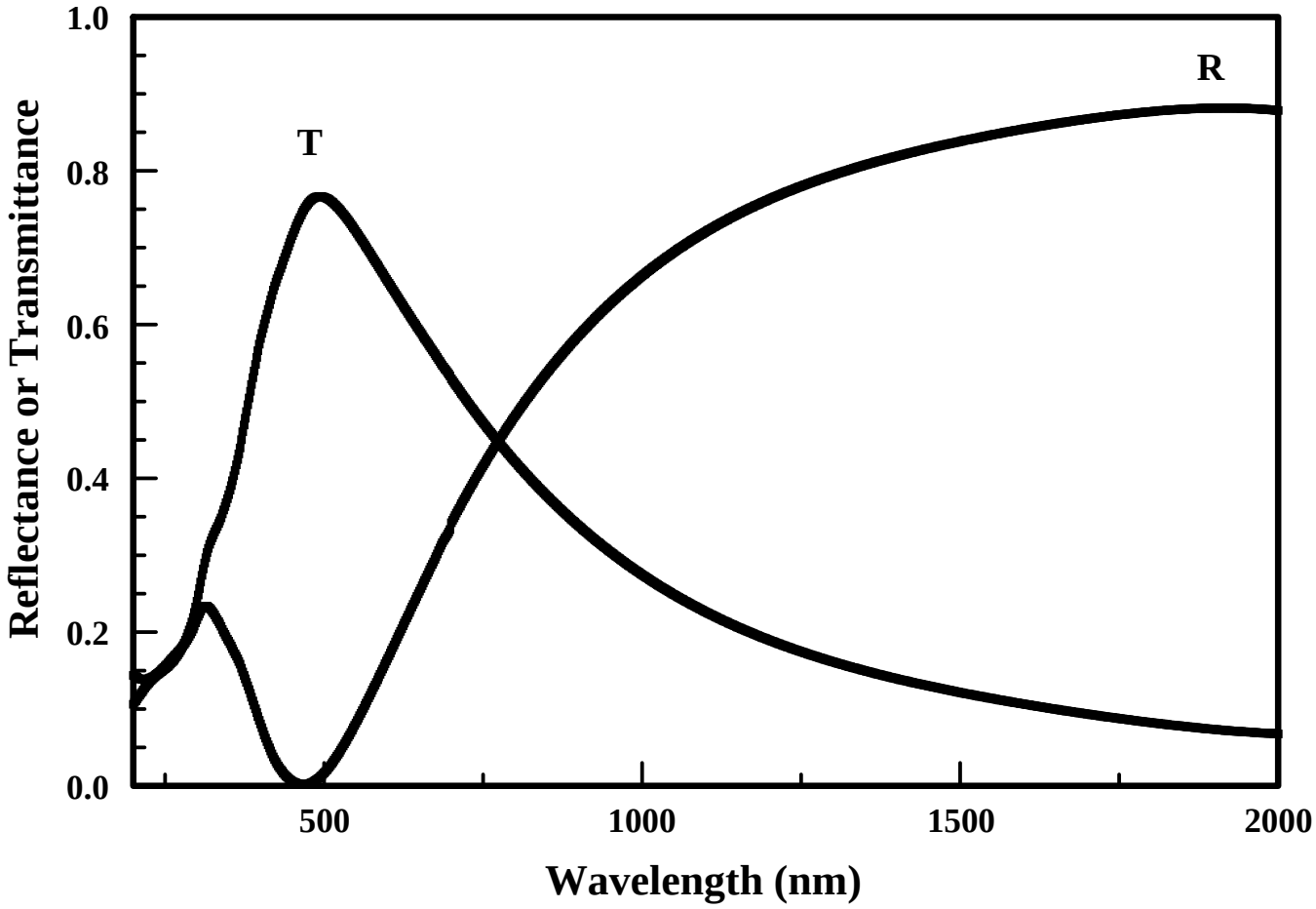

Figure 7.4 Normal-incidence transmittance and reflectance spectra of a transparent heat mirror based on the V_2O_5/Ag structure. The thickness of V_2O_5 was 40 nm, and that of silver was 40 nm.

Table 7.1 Numerical evaluation of the optical properties of the transparent heat mirrors

THM	T_{max}	λ^*_{max} (nm)	τ_{vis} (nm)	R_{IR} (nm)	Φ (nm^2)
NiO/Ag	0.692	554	188.2	1000.6	1.30×10^5
MoO_3/Ag	0.784	492	204.3	952.4	1.53×10^5
Cr_2O_3/Ag	0.693	508	188.0	1012.5	1.32×10^5
V_2O_5/Ag	0.767	494	201.3	977.1	1.51×10^5

(*) λ_{max} is the wavelength at which maximum transmittance occurs

7.2 Chemical Properties

The performance of a THM is predominantly affected by the silver layer. When the oxide layer is deposited on top of the silver layer, the silver surface is damaged to some extent [109], causing the diffusion of the oxide into the silver layer, with subsequent deterioration of the performance of the heat mirror [110]. A criterion of critical importance to the THM is its selectivity, which is degraded by the lack of sharp interfaces between the oxide and silver layers, due to the diffusion process [23]. XPS depth profiling was used to investigate the diffusion of the oxide layer into the silver layer. Figures 7.5 to 7.8 show the elemental depth profiles of the THMs, which give the spatial distribution of the elements with the thickness of the THM. These profiles were calculated from the areas of the O1s, Ag 3d, and corresponding metal peaks. The figures clearly show that the interface between the two layers was not sharp, and thus diffusion of the oxide into the silver layer took place. This diffusion may be understood on the basis of the topography of the silver layer. AFM analysis showed that the silver layer was characterized by a columnar porous structure, and such a morphology enhances the diffusion of the oxide into the silver layer.

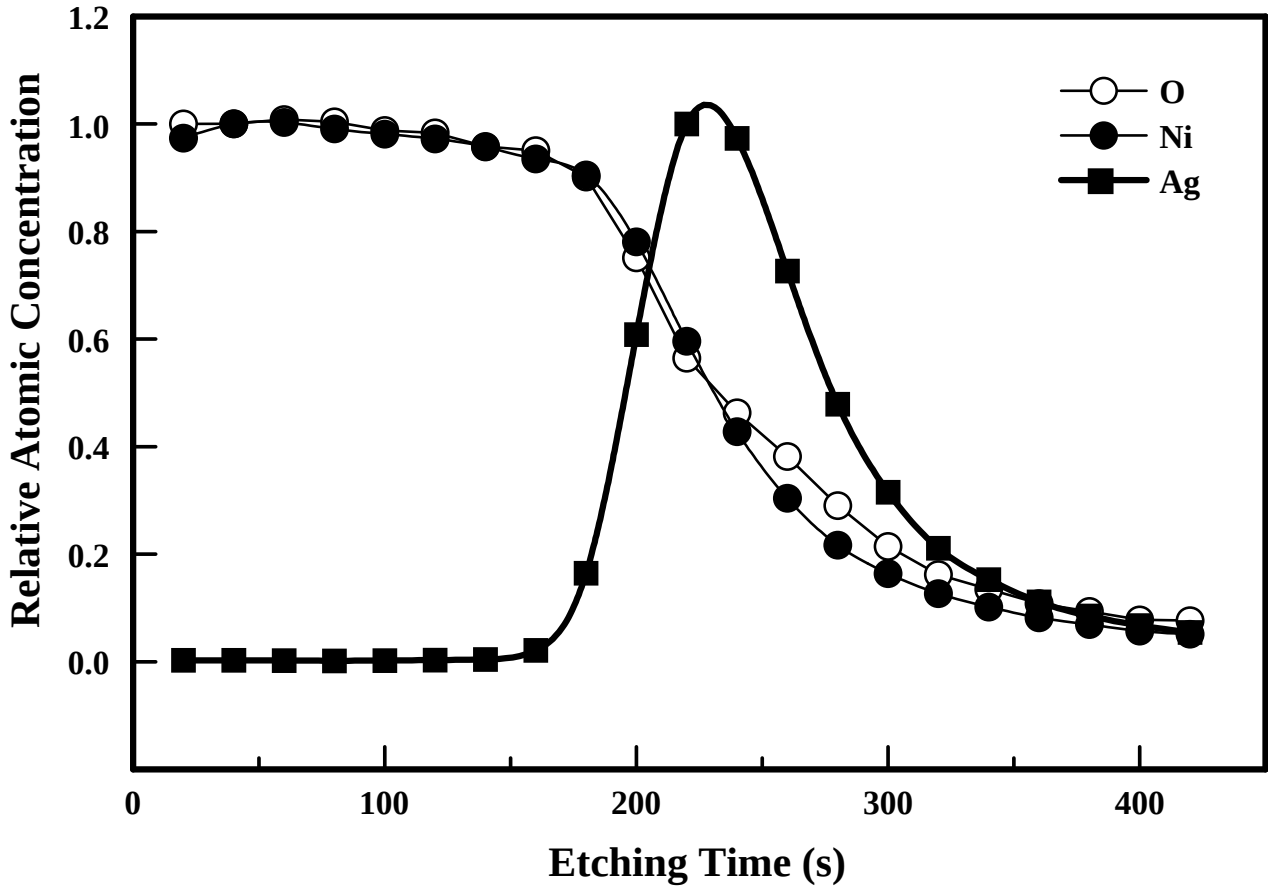

Figure 7.5 XPS depth profile spectra of the NiO/Ag THM showing the variation of the relative atomic concentration of the various elements as a function of etching time for the two-layer structure whose optical spectra are shown in Figure 7.1.

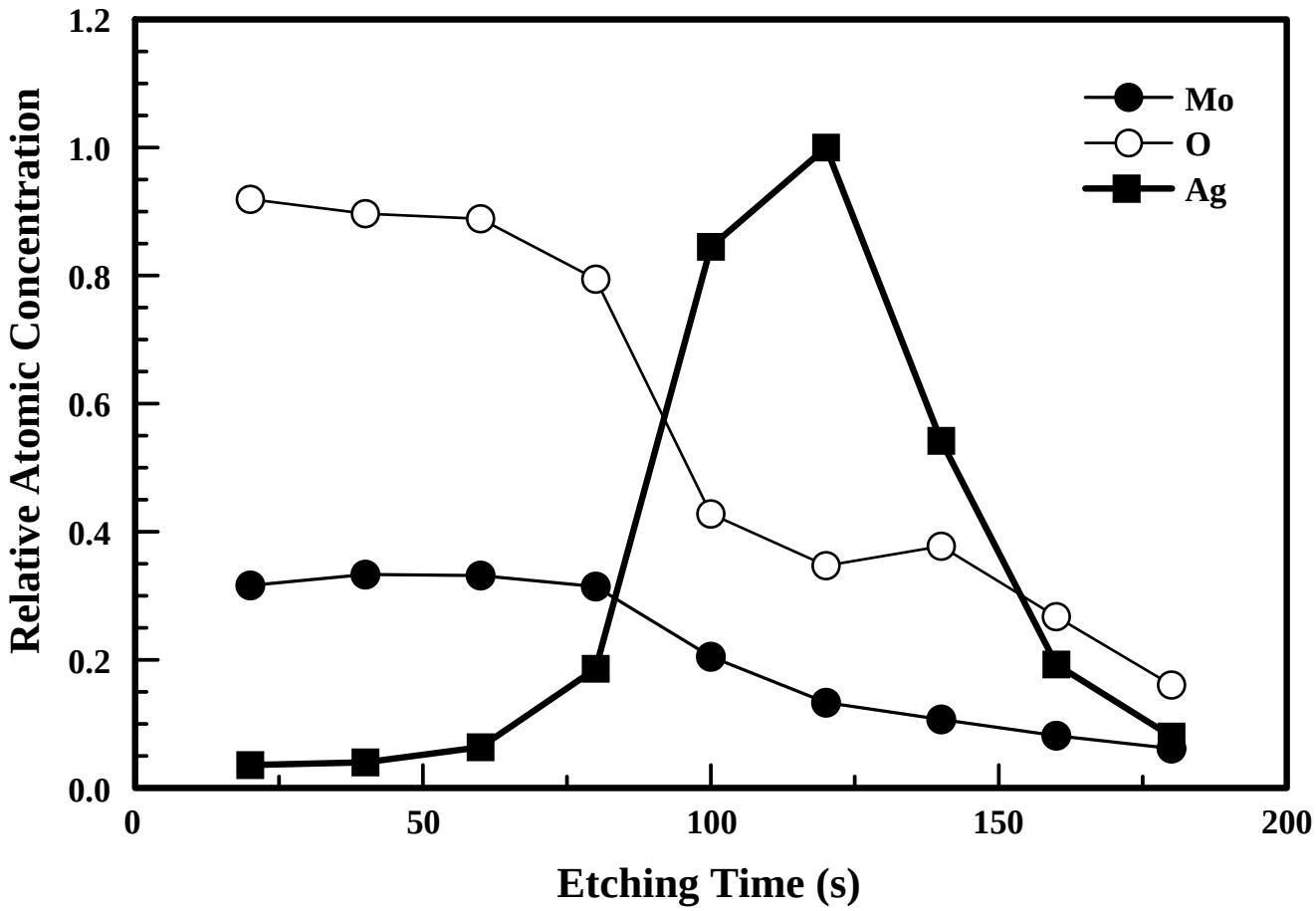

Figure 7.6 XPS depth profile spectra of the MoO3/Ag THM showing the variation of the relative atomic concentration of the various elements as a function of etching time for the two-layer structure whose optical spectra are shown in Figure 7.2.

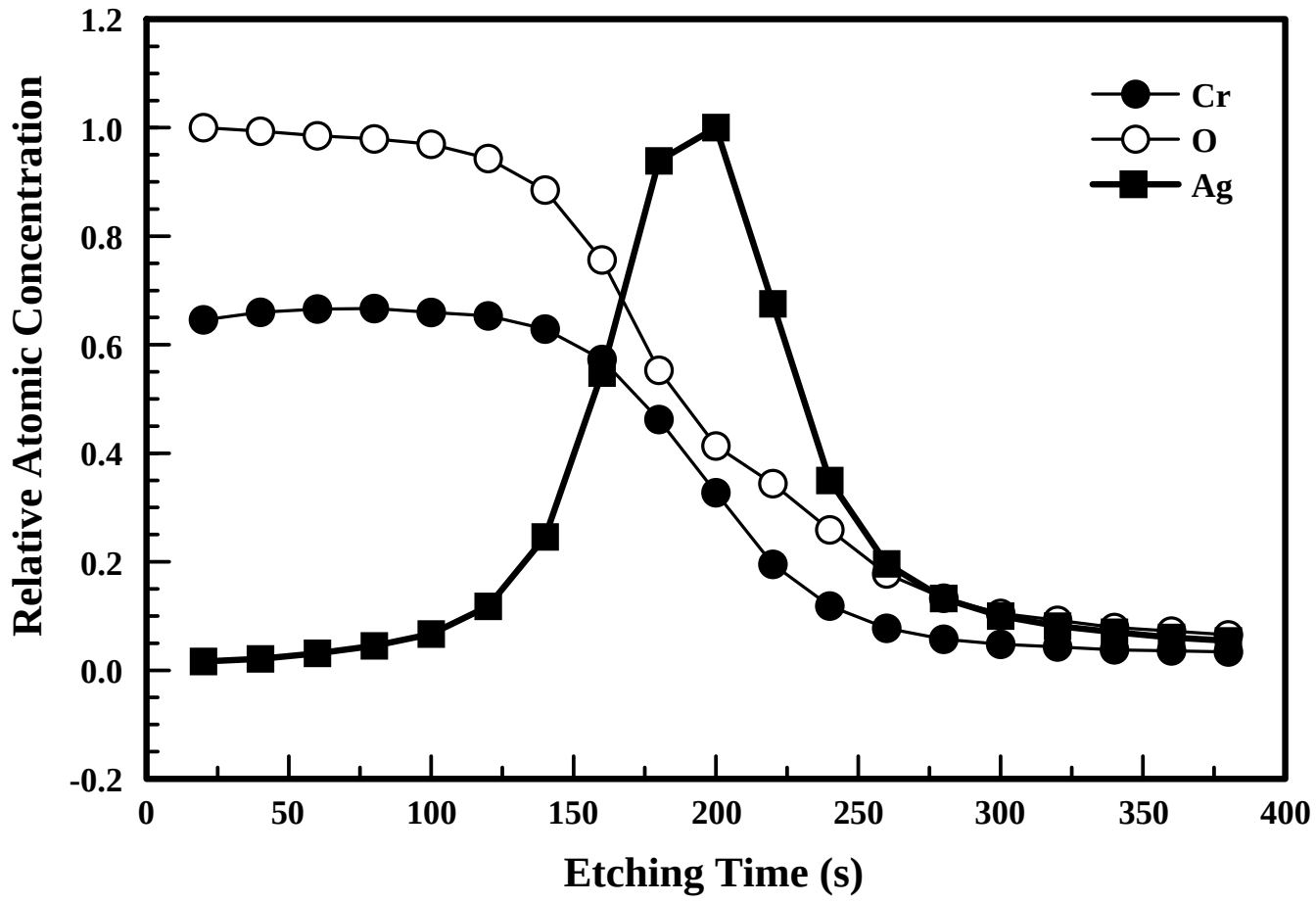

Figure 7.7 XPS depth profile spectra of the Cr2O3/Ag THM showing the variation of the relative atomic concentration of the various elements as a function of etching time for the two-layer structure whose optical spectra are shown in Figure 7.3.

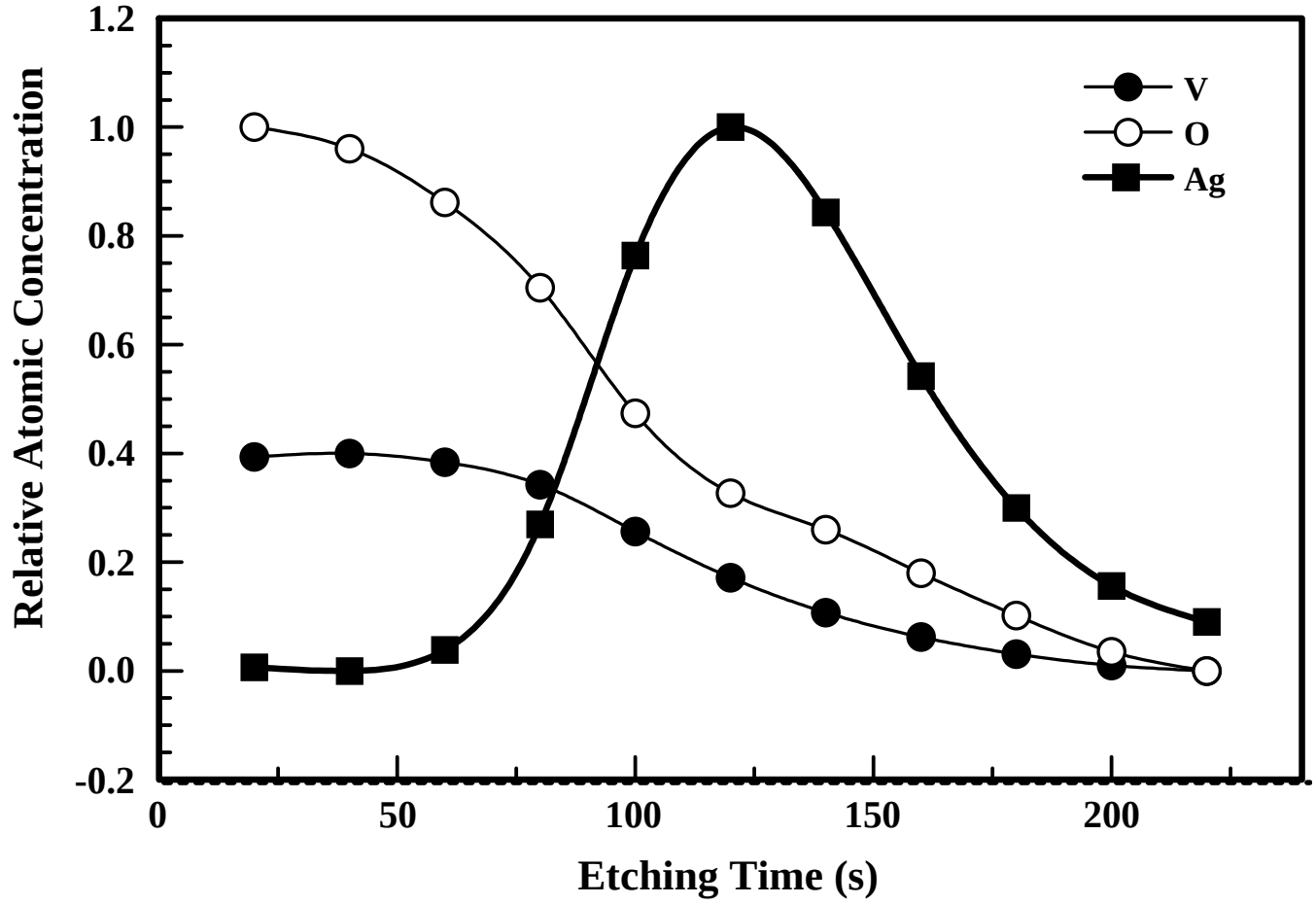

Figure 7.8 XPS depth profile spectra of the V_2O_5/Ag THM showing the variation of the relative atomic concentration of the various elements as a function of etching time for the two-layer structure whose optical spectra are shown in Figure 7.4.

7.3 Evaluation of Performance

The performance of a THM is evaluated in terms of the integrated solar (SOL) and visible (VIS) transmittance and reflectance [12,111,112]. These quantities are defined by:

$$\chi_{SOL} = \frac{\int \chi(\lambda) S(\lambda) d\lambda}{\int S(\lambda) d\lambda} \qquad \{\lambda: 400\ \text{nm-}2000\ \text{nm}\} \qquad (7.4)$$

$$\chi_{VIS} = \frac{\int \chi(\lambda) S(\lambda) \Phi(\lambda) d\lambda}{\int S(\lambda) \Phi(\lambda) d\lambda} \qquad \{\lambda: 400\ \text{nm-}700\ \text{nm}\} \qquad (7.5)$$

where χ stands for transmittance or reflectance, S is the normalized AM1 solar spectrum [113], and φ is the photopic luminous efficiency of the human eye [114]. The integrated solar and visible quantities were calculated for the THMs, and the results are listed in Table 7.2.

For optimal performance of a THM, it is indispensable to enhance the integrated visible transmittance and decrease the integrated solar transmittance to overcome over-heating [115]. Therefore, the ratio T_{vis}/T_{sol}, should be as large as possible. However, since around 50 % of the solar spectrum is in the visible range, the maximum possible value of this ratio is 2 [115]. My values for this ratio were around 1.5. This value is acceptable in view of the fact that my measurement range (0.7 to 2.0 μm) was only a small portion of the infrared range that extends from 0.7 to 25 μm.

Table 7.2 Integrated spectral quantities of the transparent heat mirrors

THM	T_{SOL}	T_{vis}	R_{SOL}	R_{vis}	T_{vis}/ T_{SOL}
NiO/Ag	0.444	0.676	0.435	0.171	1.52
MoO_3/Ag	0.474	0.716	0.370	0.096	1.51
Cr_2O_3/Ag	0.433	0.659	0.434	0.160	1.52
V_2O_5/Ag	0.478	0.704	0.384	0.102	1.47

CHAPTER 8: CONCLUSIONS

8.1 Conclusions

Transparent heat mirrors (THM) allow the visible range of electromagnetic radiation to transmit through them but reflect the infrared part. Transparent heat mirrors based on two layer Dielectric/Metal systems (D/M) were fabricated using thermal evaporation. Silver was used as metal and transition metal oxides (TMOs) chromium oxide (Cr_2O_3), molybdenum oxide (MoO_3), nickel oxide (NiO), and vanadium oxide (V_2O_5) thin films were used as the dielectrics. First, I deposited individual oxide layers and investigated their properties that are of relevance to THMs. Then, I fabricated THMs and investigated their properties. In addition, I evaluated the performance of these mirrors as required for energy-saving applications. MoO_3, Ag and V_2O_5 were deposited by thermal evaporation from resistively-heated boats, whereas NiO and Cr_2O_3 were deposited by electron-beam evaporation. Individual transition metal oxides thin films, deposited by thermal evaporation, were found to exhibit the desired properties that are necessary for their utilization in the energy-saving transparent heat mirror multilayer structures. This was manifested by their smooth and dense surfaces that had a nanometer scale surface roughness, and a columnar structure. The structural properties indicated that all the films were amorphous except those of nickel oxide. From an optical point of view, the individual transition metal oxides thin films were characterized by a high refractive index that was between 1.8 – 2.1 in the desired spectral range, and a wide band gap of the range 2.18-3.82 eV that rendered them transparent to visible radiation. Chemical depth profiling of the THMs revealed significant diffusion of transition metal oxides layer into the silver layer. This was attributed to the porous and columnar structure of the silver layer.

The chemical state and composition of the films were investigated using XPS. This technique is sensitive to core level shifts and is able to give information on the metallic environment and oxidation state. The nickel XPS 2p core level spectrum consists of two sublevels ($2p_{1/2}$ and $2p_{3/2}$) due to spin-orbit splitting. The Ni $2p_{3/2}$ spectrum is very complex due to the existence of several oxidation states, including Ni^{2+} (NiO and $Ni(OH)_2$) and Ni^{3+} (Ni_2O_3), and multiplet splitting. The first two components (A and B) were assigned to NiO. They may arise from multiplet splitting of NiO. Components C and D were assigned to $Ni(OH)_2$ and Ni_2O_3, respectively. They arise from the exposure of the films to air. The O1s spectrum was resolved into two components (A and B). The O 1s low binding- energy component (A) may be assigned to NiO. The O 1s high binding- energy component (B) may be assigned to Ni_2O_3, $Ni(OH)_2$, and adsorbed oxygen species (such as water and carbonates) that result from exposure of the films to air. The molybdenum XPS 3d core level spectrum consists of two sublevels ($3d_{3/2}$ and $3d_{5/2}$) due to spin-orbit splitting. Typically, the O ls spectrum in MoO_3 thin films consists of two components. The first component occurs on the low binding energy side in the spectrum and is called the low-binding-energy (LBE) component. This component is attributed to oxygen bound to molybdenum. The second component, high-binding-energy (HBE) component, may be attributed to oxygen species (such as water vapour, OH species, or carbonates) adsorbed at the surface of the film. The chromium XPS 2p core level spectrum consists of two sublevels ($2p_{1/2}$ and $2p_{3/2}$) due to spin-orbit splitting. The Cr $2p_{3/2}$ spectrum is very complex and asymmetric, possibly due to the existence of several oxidation states, multiplet splitting, and 3d shake-up satellites. Similarly, the O 1s core level spectrum is asymmetric due to the existence of several oxidation states and/or adsorbed oxygen species (such as water, hydroxyl group, or carbonates) that may be present at the surface of the film due to its exposure to the atmosphere. The

vanadium XPS 2p core level spectrum consists of two sublevels ($2p_{1/2}$ and $2p_{3/2}$) due to spin-orbit splitting. Similarly, the O1s core level spectrum is asymmetric due to the existence of several oxidation states and/or adsorbed oxygen species (such as water, hydroxyl group, or carbonates) that may be present at the surface of the film due to its exposure to the atmosphere.

For THM applications, it is desirable to maximize visible transmittance and infrared reflectance. It is evident (section 7.1) that the films deposited by thermal evaporation (MoO_3 and V_2O_5) showed slightly better performance than those deposited by e-beam evaporation (Cr_2O_3, and NiO). This may be attributed to the fact that there was more inter-diffusion among the layers deposited by e-beam evaporation. On the other hand, the maximum transmittance of the e-beam evaporated films was shifted to the visible range, as desired in THM applications. The complete analysis showed that MoO_3 and V_2O_5 are the best oxides for their utilization in the energy-saving transparent heat mirror multilayer structures. The solar performance of the heat mirrors was evaluated by determining the visible-to-solar transmittance ratio. The average ratio was found to be about 1.5, whereas the maximum theoretical value is 2. For optimal performance of a THM, it is indispensable to enhance the integrated visible transmittance and decrease the integrated solar transmittance to overcome over-heating. Therefore, the ratio T_{vis}/T_{sol}, should be as large as possible. It has been observed that ratio T_{vis}/T_{sol} has highest value (1.52) for Cr_2O_3, and NiO, whereas it is 1.51 and 1.47 for MoO_3 and V_2O_5, respectively.

All the transparent heat mirrors based transition metal oxides (Cr_2O_3, MoO_3, NiO, and V_2O_5) are highly energy efficient and have almost same performance. However the transparent heat mirrors deposited by thermal evaporation (MoO_3/Ag and V_2O_5/Ag) showed slightly better performance than those deposited by e-beam evaporation (Cr_2O_3/Ag and NiO/Ag).

8.2 Suggestion for further work

1. Investigate the effect of thickness of transition metal oxides layers on the properties of THM.
2. Investigate three-layer (D/M/D) structure and compare it with the double layer coatings.
3. Deposit the metal oxide films by using other techniques like spray pyrolysis, pulse laser and sputtering deposition techniques.
4. Investigate the effect of annealing and substrate temperature on the optical properties of THM.
5. Study the environmental impact on the durability of these coatings.

References

[1] P. Jin, L. Miao, S. Tanemura, G. Xu, M. Tazawa, and K. Yoshimura, “Formation and characterization of TiO_2 thin films with application to a multifunctional heat mirror”, Applied Surface Science, Vol. 212-213 (2003), pp.775-781.

[2] C. M. Lampert, “Heat mirror coatings for energy conserving windows”, Solar Energy Materials, Vol.6 (1981), pp.1-41.

[3] J.C Fan, ”Selective Black Absorbers using sputtered cermet films”, Thin Solid Films, Vol.54 (1978), pp.139-148.

[4] H. G. Craighead, R. Bartynskiand R. A. Buhrman, “Metal/Insulator composite selective absorbers”, Solar Energy Materials, Vol. 1 (1979), pp. 105-124.

[5] B. Karlsson, E. Valkonen, T. Karlsson, and C. G. Ribbing, “Materials for solar transmitting heat reflecting coatings”, Thin Solid Films,Vol.86(1981), pp.91-98.

[6] R.P Howson, J.N Avaritsiotis, M. I. Ridge, and C. A Bishop, ”Formation of transparent heat mirrors by ion plating on to ambient temperature substrates”, Thin Solid Films, Vol.63 (1979), pp.163-167.

[7] M.M Hasan, A. B. M Abdul Malek, A. S. M. A. Haseeb and H. H. Masjuki, “Investigations on TiO_2 and Ag based single and multilayer films for window glazing”, ARPN Journal of Engineering and Applied Sciences, VOL. 5 (2010), pp.22-28.

[8] C.C. Lee, S.H. Chen, and C.C. Jaing, “Optical monitoring of silver-based transparent heat mirrors”, Applied Optics, Vol. 35 (1996), pp.5698-5703.

[9] B. E. Yoldas, and T. O'Keefe, “Deposition of optically transparent IR reflective coatings on Glass”, Applied Optics, Vol.23 (1984), pp.3638-3643.

[10] M.F Al-Kuhaili, A.H. Al-Aswad, S.M.A Durrani and I.A Bakhtiari, “Transparent heat mirrors based on tungsten oxide–silver multilayer structures”, Solar Energy, Vol.83 (2009) pp.1571–1577.

[11] P. B. Johnson, and R. W. Christy, “Optical constants of the noble metals”, Physical Review B, Vol.6 (1972), pp.4370-4379.

[12] P. H. Berning, “Principles of design of architectural coatings”, Applied Optics, Vol. 22 (1983), pp.4127-4141.

[13] G. Kienel, ”Optical layers produced by sputtering”, Thin Solid Films, Vol.77 (1981), pp. 213-224.

[14] G. Leftheriotis, P. Yianoulis and D. Patrikios, “Deposition and optical properties of optimized ZnS/Ag/ZnS thin films for energy saving applications”, Thin Solid Films, Vol. 306 (1997), pp. 92-99.

[15] H. Kostlin, and G. Frank, “Optimization of transparent heat mirrors based on a thin silver film between antireflection films”, Thin Solid Films, Vol.89 (1982), pp.287-293.

[16] J. C Fan, “Sputtered films for wavelength-selective applications”, Thin Solid Films, Vol.80 (1981), pp.125-136.

[17] J.A. Pracchia, and J.M Simon, ”Transparent heat mirrors: influence ofthe materials on the optical characteristics”, Applied Optics, Vol.20 (1981), pp. 251–258.

[18] S. S Kanu and R. Binions, ”Thin films for solar control applications”, Proceeding of the Royal Society, Vol. 466A (2010), pp.19–44.

[19] C.G Granqvist,“Window coating for the future”, Thin Solid Films, Vol.193-194(1990), pp.730-741.

[20] S.M Babulanam, T.S Eriksson, G.A Niklasson, and C.G Granqvist, ”Thermochromic VO_2 films for energy efficient windows”, Solar Energy Materials, Vol. 16 (1987), pp. 347-363.

[21] H.K Koduru, H.M Obili and G. Cecilia, ”Spectroscopic and electrochromic properties of activated reactive evaporated nano-crystallineV_2O_5 thin films grown on flexible substrates”, International Nano Letters, Vol.3 (2013), pp.24.

[22] M.A. Sobhan, M.R. Islam, and K.A. Khan, “Preparation and properties of V_2O_5 thin films for energy-efficient selective-surface applications”, Applied Energy, Vol.64 (1999), pp.345-351.

[23] J.C Fan , F. L. Bachner, G. H. Foley, and P. M. Zavracky, "Transparent heat-mirror films of TiO_2/Ag/TiO_2 for solar energy collection and radiation insulation", Applied Physics Letter, Vol. 25 (1974), pp.693-695.

[24] M.F Al-Kuhaili, “Optical properties of hafnium oxide thin films and their application in energy-efficient windows”, Optical Materials, Vol. 27 (2004), pp.383–387.

[25] M.F Al-Kuhaili, A.H Al-Aswad, S.M.A. Durrani, I.A Bakhtiari, “Energy-saving transparent heat mirrors based on tungsten oxide–gold WO_3/Au/WO_3 multilayer structures”, Solar Energy, Vol.86 (2012), pp. 3183–3189.

[26] S.M.A. Durrani, E.E. Khawaja, A.M. Al-Shukri, and M.F. Al-Kuhaili, "Dielectric/Ag/dielectric coated energy-efficient glass windows for warm climates", Energy and Buildings, Vol. 36 (2004), pp. 891–898.

[27] R. P. Howson and M. I. Ridge, "Deposition of transparent heat reflecting coatings of metal oxides using reactive planar magnetron sputtering of a metal and/or alloy", Thin SolidFilms, Vol. 77 (1981), pp. 119-125.

[28] F. Simonies, E. Kauer, M. Leij and C.J hoogendoorn, "Physics of doped tin dioxide films for spectral selective surface", Solar Energy Materials, Vol. 1 (1979), pp. 221-231.

[29] G. Frank, E. Kauer and H. Kostlin, "Transparent heat reflecting coatings based on highly doped semiconductor", Thin Solid Films, Vol. 77 (1981), pp. 107-117.

[30] H. Dislich and E. Hussmann, "Amorphous and crystalline dip coatings obtained from organomatallic solutions: procedures, chemical processes and products" Thin Solid Films, Vol. 77 (1981), pp.129-139.

[31] Z.C. Jin, I. Hamberg, and C. G. Granqvist, "Optical properties of sputter deposited ZnO:Al thin films", Journal of Applied Physics, Vol. 64 (1988), pp. 5117-5131.

[32] I. Hamberg and C. G. Granqvist, "Evaporated Sn-doped In_2O_3 films: Basic optical properties and applications to energyefficient windows", Journal of Applied Physics, Vol. 60 (1986), pp. R123-R159.

[33] S. Takaki, K. Matsumoto and K. Suzuki, "Properties of highly conducting ITO films prepared by Ion Plating", Applied Surface Science, Vol. 33/34 (1988), pp. 919-925.

[34] H. Haitjema, J.J Ph.Elich and C.J Hoogendoorn, "The optical, electrical and structural properties of fluorine-doped, pyrolytically sprayed tin oxide coatings", Solar energy Materials, Vol. 18 (1989), pp. 283-297.

[35] M.H Gitlitz, R. Dirkx, and D.A Russo , "Letting light in, keeping heat out", Chemtech, Vol. 22(1992), pp. 552-556.

[36] H. Dewaal and F. Simonis, "Tin oxide coatings: physical properties and applications", Thin Solid Films, Vol. 77 (1981), pp. 253-258.

[37] H.L Hartnagel, A.L Dawar, A.K Jain, and C Jagadish, "*Semiconducting Transparent Thin Films"*, IOP publishing, 1st Edition , Bristol, 1995.

[38] K.S SreeHarsha, "*Principles of Physical Vapor Deposition of Thin Films*", Elsevier Publishing, 1st Edition, Oxford, 2006.

[39] K.L. Chopra, "*Thin Film Phenomena*", McGraw-Hill publishing, New York (1969).

[40] N.W. Ashcroft, and N.D. Mermin, *"Solid State Physics"*, Brooks/Cole Cengage Learning, 1976.

[41] E. Meyer, "Atomic Force Microscopy", Progress in Surface Science, Vol. 41 (1992), pp. 3-49.

[42] R. Paynter, *"*XPS Theory", John Wiley and Sons, New York, 2000.

[43] N. Winograd, and S.W Gaarenstoorm, "X-ray Photoelectron Spectroscopy", Physical Methods in Modern Chemical Analysis, Vol.2 (1980), pp. 116-152.

[44] C.R Brundal, and A.D Baker, *"Electron Spectroscopy: Theory, Techniques and Applications"*, Academic Press, Vol.2, London (1978).

[45] G. A. Nicklasson, C. G. Granqvist, “Electrochromics for smart windows: thin films of tungsten oxide and nickel oxide, and devices based on them”, Journal of Material Chemistry, Vol.17 (2007), pp.127-156.

[46] S. Seo, M. J. Lee, D. H. Seo, E. J. Jeoung, D. S. Suh, Y. S. Joung, I. K. Yoo, I. R. Hwang, S. H. Kim, I. S. Byun, J. S. Kim, 1. S. Choi, and B. S. Park, “Reproducible resistance switching in polycrystalline NiO films”, Applied Physics Letter, Vol. 85 (2004), pp.5655-5657.

[47] I. Hotovy, J. Huran, P. Siciliano, S. Capone, L. Spiess, V. Rehacek, “The influence of preparation parameters on NiO thin film properties for gas-sensing applications”, Sensors & Actuators B, Vol. 78 (2001), pp.126-132.

[48] L. Ai, G. Fang, L. Yuan, N. Liu, M. Wang, C. Li, Q. Zhang, J. Li, X. Zhao, “Influence of substrate temperature on electrical and optical properties of p-type semitransparent conductive nickel oxide thin films deposited by radio frequency sputtering”, Applied Surface Science, Vol.254 (2008), pp. 2401-2405.

[49] S. Nandy, U. N. Maiti, C. K. Ghosh, and K. K. Chattopadhyay, “Enhanced p-type conductivity and band gap narrowing in heavily Al doped NiO thin films deposited by RF magnetron sputtering”, Journal of Physics: Condense Matter, Vol. 21 (2009), Art.No. 115804.

[50] K. Xerxes Steirer, J. P. Chesin, N. E. Widjonarko, J. J. Berry, A. Miedaner, D. S. Ginley, and D. C. Olson, “Solution deposited NiO thin-films as hole transport layers in organic photovoltaics”, Organic Electronics Journal,Vol.11 (2010), pp.1414-1418.

[51] G. H. Guai, M. Y. Leiw, C. M. Ng, C. M. Li, “Sulfur-doped nickel oxide thin film as alternative to Pt for dye-sensitized solar cell counter electrodes”, Advance Energy Materials, Vol. 2 (2012), pp.334-338.

[52] S. Oswald, and W. Bruckner, “XPS depth profile analysis of non-stoichiometric NiO films”, Surface and Interface Analysis, Vol. 36 (2004), pp.17-22.

[53] J. L. Yang, Y. S. Lai, and L. S. Chen, “Effect of heat treatment on the properties of non-stoichiometric p-type nickel oxide films deposited by reactive sputtering”, Thin Solid Films, Vol.488 (2005), pp.242-246.

[54] B. Subramanian, M. M. Ibrahim, V. Senthilkumar, K. R. Murali, V. Vidhya,C. Sanjeeviraja, and M. Jayachandran, “Optoelectronic and electrochemical properties of nickel oxide (NiO) films deposited by DC reactive magnetron sputtering”, Physics B, Vol. 403 (2008), pp.4104-4110.

[55] J. K. Kang, and S. W. Rhee, “Chemical vapor deposition of nickel oxide films from Ni $(C_5H_5)_2/O_2$”, Thin Solid Films, Vol. 391(2001), pp.57-61.

[56] H. L. Lu, G. Scarel, M. Alia, M. Fanciulli, S. 1. Ding, and D. W. Zhang, “Spectroscopic ellipsometry study of thin NiO films grown on Si(l00) by atomic layer deposition”, Applied Physics Letter, Vol. 92 (2008), Art.No. 222907.

[57] I. Porqueras, and E. Bertran, ” Electrochromic behaviour of nickel oxide thin films deposited by thermal evaporation”, Thin Solid Films, Vol.398 –399 (2001), pp.41–44.

[58] D.Y. Jiang, J.M. Qin, X. Wang, S. Gao, Q.C. Liang, and J.X. Zhao, ” Optical properties of NiO thin films fabricated by electron beam evaporation”, Vacuum, Vol.86 (2012), pp.1083-1086.

[59] S. Zhao, C. G. Ribbing, E. Wackelgard, “Optical constants of sputtered Ni/NiO solar absorber film - depth-profiled characterization”, Solar Energy Materials and Solar Cells, Vol. 84 (2004), pp.193-203.

[60] ICDD files: (00-001-1239) for nickel oxide; and (00-001-1167) for silver.

[61] R. Brenier, J. Mugnier, E. Mirica, "XPS study of amorphous zirconium oxide prepared by sol-gel", Applied Surface Science, Vol. 143 (1999)pp. 85-118.

[62] M. T. Greiner, M. G. Helander, Z. B. Wang, W. M. Tang, and Z. H. Lu, "Effects ofprocessing conditions on the work function and energy-level alignment of NiO thin films", Journal of Physical Chemistry C, Vol. 114(2010) pp.19777-19781.

[63] O. S. Heavens, “Optical Properties of Thin Solid Films”, Dover (1991).

[64] J. C. Manifacier, 1. Gasiot, 1. P. Fillard, “A simple method for the determination of the optical constants n, k and the thickness of a weakly absorbing thin film”, Journal of Physics E, Vol. 9(1976) pp.1002-1004.

[65] W.M Haynes, *“Hand Book of Chemistry and Physics”,* CRC Press, Boca Raton, FL, (2005).

[66] C. V. Raman, C. M. Julien, “Chemical and electrochemical properties of molybdenum oxide thin films prepared by reactive pulsed laser assisted deposition”, Chemical Physics Letter, Vol. 428 (2006), pp. 114-118.

[67] A. Szekeres, T. Ivanova, and K. Gesheva, "Spectroscopic ellipsometry study of CVD molybdenum oxide films: effect of temperature", Journal of Solid State Electrochemistry, Vol. 7 (2002), pp. 17-20.

[68] T. Aoki, T. Matsushita, K. Mishiro, A. Suzuki, and M. Okuda, "Optical recording characteristics of molybdenum oxide films prepared by pulsed laser deposition method", Thin Solid Films, Vol. 517 (2008), pp. 1482-1486.

[69] M. Arita, H. Kaji, T. Fujii, and Y. Takahashi, "Resistance switching properties of molybdenum oxide films", Thin Solid Films, Vol. 520 (2012), pp. 4762-4767.

[70] G. Zhao, N. Zhang, and K. Sun, "Porous MoO_3films with ultra-short relaxation time used for supercapacitors", Material Research Bulletin, Vol. 48 (2013), pp. 1328-1332.

[71] O.M. Hussain, and K.S. Rao,” *Characterization of activated reactive evaporated MoO3 thin films for gas sensor applications*”, Materials Chemistry and Physics, Vol.80 (2003), pp. 638–646.

[72] G. Fu, X. Xu, X. Lu, and H. L. Wan, "Mechanisms of methane activation and transformation on molybdenum oxide based catalysts", Journal of American Chemical Society, Vol. 127 (2005), pp.3989-3996.

[73] L. Q. Mai, B. Hu, W. Chen, Y. Y. Qi, C. S. Lao, C. Lao, R. S. Yang, Y. Dai, and Z. L. Wang, "Lithiated MoO_3 nanobelts with greatly improved performance for lithium batteries", Advance Materials, Vol. 19 (2007), pp. 3712-3716.

[74] C. Girotto, E. Voroshazi, D. Cheyns, P. Heremans, and B. P. Rand, "Solution-processed MoO3 thin films as a hole-injection layer for organic solar cells", ACS Applied Materials and Interfaces, Vol. 3 (2011), pp. 3244-3247.

[75] A. Siokou, G. Leftheriotis, S. Papaefthimiou, and P. Yianoulis, "Effect of the tungsten and molybdenum oxidation states on the thermal coloration of amorphous WO_3 and MoO_3 films", Surface Science,Vol. 482-485 (2001), pp. 294-299.

[76] T. S. Sian, and G.B. Reddy,” Optical, structural and photoelectron spectroscopic studies on amorphous and crystalline molybdenum oxide thin films”, Solar Energy Materials & Solar Cells, Vol.82 (2004), pp.375–386

[77] S. H. Mohamed, O. Kappertz, J. M. Ngaruiya, T. P. Leervad Pedersen, R. Drese, and M. Wuttig, "Correlation between structure, stress and optical properties in direct current sputtered molybdenum oxide films", Thin Solid Films, Vol. 429 (2003), pp.135-143.

[78] C. V. Ramana, V. V. Atuchin, V. G. Kesler, V. A. Kochubey, L. D. Pokrovsky, V. Shutthanandan, U. Becker, and R. C. Ewing, "Growth and surface characterization of

sputter-deposited molybdenum oxide thin films", Applied Surface Science, Vol. 253 (2007), pp. 5368-5374.

[79] M. Diskus, O. Nilsen, and H. Fjellvag, Growth of thin films of molybdenum oxide by atomic layer deposition, Journal of Material Chemistry, Vol.21 (2011), pp. 705-710.

[80] Refractive Index Database: http://refractiveindex.info/

[81] PM. Sousa, AG. Silvestre, and O. Conde, "Cr_2O_3 thin films grown at room temperature by low pressure chemical vapor deposition." Thin Solid Films, Vol. 519 (2011), pp. 3653-3657.

[82] G. Carta, MN Rossetto, P. Zanella, G. Salmaso, S. Restello, V. Rigato, S. Kaciulis, and A. Mezzi , "A comparative study of Cr_2O_3 thin films obtained by MOCVD using three different precursors." Chemical Vapor Deposition, Vol. 11 (2005), pp. 375-380.

[83] P. Hones, M. Diserens, and F. Levy, "Characterization of sputtered-deposited chromium oxide thin films", Surface Coating Technolology, Vol. 120-121 (1999), pp. 277-283.

[84] I. Ivanova, K. Gesheva, P. Sharlandjiev, and K. Georgieva, "Technology and optoelectronic properties of APCVD Cr_2O_3 and Mo-Cr mixed oxide thin films", Surface Coating Technolology, Vol. 201 (2007), pp. 9313-9318.

[85] N. Popovici, ML. Parames, Da Silva, O. Monnereau, PM. Sousa, AJ. Silvestre, and O. Conde, "KrF pulsed laser deposition of chromium oxide thin films from Cr_8O_{21} targets", Applied Physics A, Vol. 79 (2004), pp. 1409-1411.

[86] T. Ivanova, M. Surtchev, and K. Gesheva, "Characterization of CVD chromium oxide thin films." Physica Status Solidi A, Vol. 184 (2001), pp. 507-513.

[87] P. Qin, G. Fang, N. Sun, X. Fan , Q. Zheng, F. Chen, J. Wan, X. Zhao, "Organic solar cells with p-type amorphous chromium oxide film as hole-transporting layer." Thin Solid Films, Vol. 519 (2011), pp. 4334-4341.

[88] RE. Kirby, EL. Garwin, FK. King, AR. Nyaiesh AR, "Surface properties of Cr_2O_3" Journal of Applied Physics, Vol. 62 (1987), pp. 1400-1405.

[89] A. V. Naumkin, A. Kraut-Vass, S. W. Gaarenstroom, and C. J. Powell, "NIST X-ray Photoelectron Spectroscopy Database", National Institute of Standards and Technology (NIST), (http://srdata.nist.gov/xps).

[90] G. Goodlet, S. Faty, S. Cardoso, P. P. Freitas, A. M. Simoes, M. G. Ferreira, and M. D. Belo, "The electronic properties of sputtered chromium and iron oxide films", Corrosion Science, Vol. 46 (2004), pp. 1479-1499.

[91] M.F Al-Kuhaili, E.E. Khawaja, D.C. Ingram, and S.M.A. Durrani, "A study of thin films of V_2O_5 containing molybdenum from an evaporation boat", Thin Solid Films, Vol. 460 (2004), pp. 30–35.

[92] X. Wu, F. Lai, L. Lin, Y. Li, Lianghui Lin, Y. Qu, and Z. Hu, "Influence of thermal cycling on structural, optical and electrical properties of vanadium oxide thin films", Applied Surface Science, Vol. 255 (2008), pp. 2840‑2844.

[93] C.E Patil, N.L Tarwal, P.S Shinde, H.P Deshmukh and P.S Patil, "Synthesis of electrochromic vanadium oxide by pulsed spray pyrolysis technique and its properties", Journal of applied Physics D, Vol. 42 (2009) , pp.1-7.

[94] M. Benmoussa, E. Ibnouelghazi, A. Bennouna, E.L. Ameziane, "Structural, electrical and optical properties of sputtered vanadium pentoxide thin films", Thin Solid Films, Vol. 265 (1995), pp. 22-28.

[95] C.V. Ramana, O.M. Hussain, S. Uthanna, and B.S Naidu, "Influence of oxygen partial pressure on the optical properties of electron beam evaporated vanadium pentoxide thin film", Optical Materials, Vol. 10 (1998), pp. 101–107.

[96] H.A Mohamed, "Sintering process and annealing effect on some physical properties of V_2O_5 thin films", Optoelectronics and advanced Materials-Rapid Communications, Vol. 3, (2009), pp. 693 – 699.

[97] C.V Ramana, O.M. Hussain, B.S Naidu, C. Julien, and M. Balkanski, "Physical investigations on electron-beam evaporated vanadium pentoxide films", Materials Science and Engineering B, Vol. 52 (1998), pp. 32–39.

[98] D. Barreca, L. Armelao, F. Caccavale, V.D Noto, A. Gregori, G.A Rizzi, and E. Tondello, "Highly oriented V_2O_5 nanocrystalline thin films by plasma-enhanced chemical vapor deposition", Chemical Materials, Vol. 12 (2000), pp. 98-103.

[99] C.V Ramana, O.M Hussain, B.S Naidu, and P.J Reddy, "Spectroscopic characterization of electron-beam evaporated V_2O_5 thin films", Thin Solid Films, Vol. 305 (1997), pp. 219-226.

[100] R.T.R Kumar, B. Karunagaran, S. Venkatachalam, D. Mangalaraj, S.K. Narayandass, and R. Kesavamoorthy, "Influence of deposition temperature on the growth of vacuum evaporated V_2O_5 thin films", Materials Letters, Vol. 57 (2003), pp. 3820–3825.

[101] R.T.R Kumar, B. Karunagaran, V. Senthil Kumar, Y.L Jeyachandran, D. Mangalaraj, and S.K. Narayandass, " Structural properties of V_2O_5 thin films prepared by vacuum evaporation ", Materials Science in Semiconductor Processing, Vol. 6 (2003), pp.543–546.

[102] L.J Meng, R.A Silva, H.N Cui, V. Teixeira, M.P. dos Santos, and Zheng Xu, " Optical and structural properties of vanadium pentoxide films prepared by d.c. reactive magnetron sputtering", Thin Solid Films, Vol. 515 (2006), pp.195 – 200.

[103] A.A Bahgat, F.A Ibrahim, and M.M El-Desoky, "Electrical and optical properties of highly oriented nanocrystalline vanadium pentoxide", Thin Solid Films, Vol. 489 (2005), pp. 68 – 73.

[104] F.N Dultsev, L.L Vasilieva, S.M Maroshina, and L.D Pokrovsky, " Structural and optical properties of vanadium pentoxide sol–gel films", Thin Solid Films, Vol. 510 (2006), pp.255 – 259.

[105] C.V Ramana, O.M Hussain, R. Pinto, and C.M. Julien, " Microstructural features of pulsed-laser deposited V_2O_5 thin films", Applied Surface Science, Vol. 207 (2003), pp.135–138.

[106] S.A Lawton, and E.A Theby, "Synthesis of vanadium oxide powders by evaporation of decomposition of solutions", Journal of American Ceramic Society, Vol. 78 (1995), pp. 104-108.

[107] M.C Biesinger, L.W.M Lau, A.R Gerson, and R.St.C. Smart, "Resolving surface chemical states in XPS analysis of first row transition metals, oxides and hydroxides: Sc, Ti, V, Cu and Zn", Applied Surface Science, Vol. 257 (2010), pp. 887–898.

[108] J. C. Parker and D. J. Lam, "Optical properties of vanadium pentoxide determined from ellipsometry and band-structure calculations", Physical Review B, Vol. 42 (1990) pp.5289-5293.

[109] K. Chiba, and K. Suzuki, "Effects of heterogeneous metal atoms on the stability of a silver layer of a heat mirror coating", Solar Energy Material & Solar Cells, Vol. 25 (1992) pp.113-123.

[110] K. Chiba, and K. Nakatani, "Photoenhanced migration of silver atoms in transparent heat mirror coatings", Thin Solid Films, Vol. 112 (1984) pp.359-367.

[111] G. B. Smith, G. A. Niklasson, J. S. E. M. Svensson, and C. -G. Granqvist, "Noble-metal-based transparent infrared reflectors: Experimental and theoretical analyses for very thin gold films", Journal of Applied Physics, Vol. 59 (1986) pp.571-581.

[112] E. Valkonen, B. Karlsson, and C. -G. Ribbing, "Solar optical properties of thin films ofCu,Ag, Au, Cr, Fe, Co, Ni and Al", Solar Energy, Vol. 32 (1984) pp.211-222.

[113] A. A. Sayigh, "Solar Energy Engineering", Academic Press, New York (1977).

[114] S.L. Williamson, H. Z. Cummins, "Light and Color in Nature and Art", Wiley (1983).

[115] K. E. Andersson, M. Veszelei, and A. Roos," Zirconium nitride based transparent heat mirror coatings - preparation and characteristics", Solar Energy Material & SolarCells, Vol. 32, (1994) pp.199-212.

Vitae

Name	Syed Haseeb Ali Ahmad
Nationality:	Pakistani
Date of Birth:	31-03-1982
Email:	active7135@gmail.com ; haseebali@kfupm.edu.sa
Permanent Address:	Village & Post Office Jamalpur Syedan, Tehsil & district Gujrat, Pakistan.

Education

1. MS Physics, 2015, Department of Physics, King Fahd University of Petroleum and Minerals (KFUPM), Dhahran, Saudi Arabia.
2. M.Sc Physics, 2009, Department of Physics, University of the Punjab, Lahore, Pakistan.
3. B.Sc Physics & Mathematics, 2007, University of the Punjab, Lahore, Pakistan.
4. DAE Electronics Engineering (Diploma of Associate Engineer), 2002, Swedish Pakistani institute of technology, Gujrat, Pakistan.

Experience

1. Research Assistant (2013-2015), Department of Physics, King Fahd University of Petroleum and Minerals (KFUPM), Dhahran, Saudi Arabia.
2. Assistant Manager, Scientist (2009-2013), Satellite Research and Development Centre, SUPARCO (Space and Upper Atmosphere Research Commission), Lahore, Pakistan.
3. Assistant Control Maintainer (2003-2009), Instrumentation & Control/ System Engineering Department, CHASNUPP (Chashma Nuclear Power Plant), Mainwali.

Publications

1. M. F. AI-Kuhaili, **S. H. A. Ahmad**, S. M. A. Durrani, M. M. Faiz, and A. UI-Hamid, "Energy-saving spectrally-selective coatings based on MoO3/Ag thin films", **Materials and Design**, Vol. 73 (2015) pp. 15–19.
2. **S. H. A. Ahmad**, M. F. AI-Kuhaili, S. M. A. Durrani, M. M. Faiz, and A. UI-Hamid, "Transparent heat mirrors based on chromium oxide thin films" (submitted)
3. M. F. AI-Kuhaili, **S. H. A. Ahmad**, S. M. A. Durrani, M. M. Faiz, and A. UI-Hamid, "Application of nickel oxide thin films in NiO/Ag multilayer energy-efficient coatings", **Material Science in Semiconductor Processing** (accepted)
4. **S. H. A. Ahmad**, M. F. AI-Kuhaili, S. M. A. Durrani, M. M. Faiz, and A. UI-Hamid, "Heat mirrors and energy efficient coatings based on vanadium oxide" (under process)